Aus dem Pathologischen Institut der Ludwig-Maximilians-Universität München

Direktor: Prof. Dr. med. Thomas Kirchner

Arbeitsgruppe Experimentelle und Molekulare Pathologie

Leiter: Prof. Dr. rer. nat. Heiko Hermeking

Genetic analysis of *miR-34a* and *miR-34b/c* functions in a mouse model of familial adenomatous polyposis

Dissertation

zum Erwerb des Doktorgrades der Naturwissenschaften (Dr. rer. nat.)

an der Medizinischen Fakultät

der Ludwig-Maximilians-Universität München

vorgelegt von

Longchang Jiang

aus

Heilongjiang, Volksrepublik China

2017

Gedruckt mit Genehmigung der Medizinischen Fakultät

der Ludwig-Maximilians-Universität München

Berichterstatter:

Prof. Dr. rer. nat. Heiko Hermeking

Zweitgutachter:

Prof. Dr. rer. nat. Peter Jon Nelson

Dekan:

Prof. Dr. med. dent. Reinhard Hickel

Tag der mündlichen Prüfung:

16.11.2017

Eidesstattliche Versicherung

Ich erkläre hiermit an Eides statt,

dass ich die vorliegende Dissertation mit dem Thema

„**Genetic analysis of *miR-34a* and *miR-34b/c* functions in a mouse model of familial adenomatous polyposis**"

selbständig verfasst, mich außer der angegebenen keiner weiteren Hilfsmittel bedient und alle Erkenntnisse, die aus dem Schrifttum ganz oder annähernd übernommen sind, als solche kenntlich gemacht und nach ihrer Herkunft unter Bezeichnung der Fundstelle einzeln nachgewiesen habe.

Ich erkläre des Weiteren,dass die hier vorgelegte Dissertation nicht in gleicher oder in ähnlicher Form bei einer anderen Stelle zur Erlangung eines akademischen Grades eingereicht wurde.

München, den_____

Longchang Jiang

Parts of this thesis have been published in:

Original article:

- **Jiang L** and Hermeking H (2017) miR-34a and miR-34b/c suppress intestinal tumorigenesis. *Cancer Research* **77**: 2746-2768

Review article:

- Rokavec M, Li H, **Jiang L** and Hermeking H (2014) The p53/miR-34 axis in development and disease. *Journal of Molecular Cell Biology* **6**: 214-230

- Rokavec M, Li H, **Jiang L** and Hermeking H (2014) The p53/microRNA connection in gastrointestinal cancer. *Clinical and Experimental Gastroenterology* **7**: 395-413

In addition, I contributed to the following original articles:

- Li H, Rokavec M, **Jiang L**, Horst D and Hermeking H (2017) Antagonistic Effects of p53 and HIF1A on microRNA-34a Regulation of PPP1R11 and STAT3 and Hypoxia-induced Epithelial to Mesenchymal Transition in Colorectal Cancer Cells. *Gastroenterology* doi: 10.1053/j.gastro.2017.04.017. [Epub ahead of print]

- Rokavec M, Oner MG, Li H, Jackstadt R, **Jiang L**, Lodygin D, Kaller M, Horst D, Ziegler PK, Schwitalla S, Slotta-Huspenina J, Bader FG, Greten FR and Hermeking H (2014) IL-6R/STAT3/miR-34a feedback loop promotes EMT-mediated colorectal cancer invasion and metastasis. *The Journal of Clinical Investigation* **124**: 1853-1867

- Cheng CY, Hwang CI, Corney DC, Flesken-Nikitin A, **Jiang L**, Oner GM, Munroe RJ, Schimenti JC, Hermeking H and Nikitin AY miR-34 cooperates with p53 in suppression of prostate cancer by joint regulation of stem cell compartment. *Cell Reports* **6**: 1000-1007

Table of Contents

Abbreviations

Abbreviation	Abbreviation Description
ABC	Avidin-Biotin Complex
APC	Adenomatous polyposis coli gene
APS	Ammonium peroxodisulfate
CLSM	Confocal laser scanning microscopy
COAD	Colon adenocarcinomas
CpG	Cytosine phosphate guanidine
CRC	Colorectal cancer
CSC	Cancer stem cell
Cy3	Cyanine 3
DAB	3, 3-diaminobenzidine
DAPI	4', 6-diamidino-2-phenylindole
DEPC	Diethyl Pyrocarbonate
DIG	Digoxigenin
DMEM	Dulbecco's modified eagle medium
DMSO	Dimethyl sulfoxide
DNA	Deoxyribonucleic acid
DOX	Doxycycline
dNTP	Deoxynucleotides triphosphate
E.coli	*Escherichia coli*
ECL	Electrochemiluminescence
ECM	Extracellular matrix
EDTA	Ethylenediaminetetraacetic acid
EGF	Epidermal growth factor
EMT	Epithelial mesenchymal transition
FBS	Fetal bovine serum
FFPE	Formalin-fixed paraffin-embedded
FISH	Fluorescence *in situ* hybridization
FITC	Fluorescein
GDC	Genomic data commons
GFP	Green fluorescent protein
GO	Gene Ontology
GSEA	Gene Set Enrichment Analysis

Abbreviation	Abbreviation Description
H&E	Hematoxylin and eosin
HBSS	Hank's balanced salt solution
HRP	Horseradish peroxidase
IEC	Intestinal epithelial cell
IHC	Immunohistochemistry
IPSC	Induced pluripotent stem cell
lncRNA	Long non-coding RNA
ISC	Intestinal stem cell
ISH	*In situ* hybridization
IVC	Individually ventilated cages
KEGG	Kyoto Encyclopedia of Genes and Genomes
MAPK	Mitogen-activated protein kinase
miRNA	Micro RNA
mRNA	Messenger RNA
Neo	Neomycin
NGS	Next-generation sequencing
ORF	Open reading frame
PAS	Periodic acid–Schiff
PBS	Phosphate-buffered saline
PFA	Paraformaldehyde
PI3K	Phosphoinositide 3-kinase
RTK	Receptor tyrosine kinases
RNA	Ribonucleic acid
SDS	Sodium dodecyl sulfate
SSC	Saline-sodium citrate
STR	Short tandem repeat
TBST	Tris-buffered saline with 0.1% Tween 20
TCGA	The Cancer Genome Atlas
TEMED	Tetramethylethylenediamine
UTR	Untranslated region
WB	Western blotting

1. Introduction

1.1 Cancer: a primer

Cancer is a major health problem worldwide. Only in 2012, approximately 14.1 million patients were diagnosed with and 8.2 million people died from cancer [1]. Tumorigenesis is a multistep process during which several oncogenes are activated and tumor-suppressor genes are inactivated by genetic or epigenetic mechanisms [2,3]. This mechanism was initially described for colorectal cancer (CRC) [4] (Figure 1). Oncogenes and tumor-suppressor genes encode proteins and microRNAs that affect numerous cellular processes. Oncogenes are often mutated or highly expressed in cancer cells. Tumor-suppressor genes negatively regulate the cell cycle and promote apoptosis, thereby preventing the transformation of normal to cancer cells. MicroRNAs regulate gene expression by binding to target mRNAs, which blocks protein translation or causes degradation of the target mRNA. Tumor suppressive miRNAs suppress the expression of mRNAs, which encode oncogenic proteins. In case these miRNAs are down-regulated or inactivated the respective target oncogenes show elevated expression [5,6].
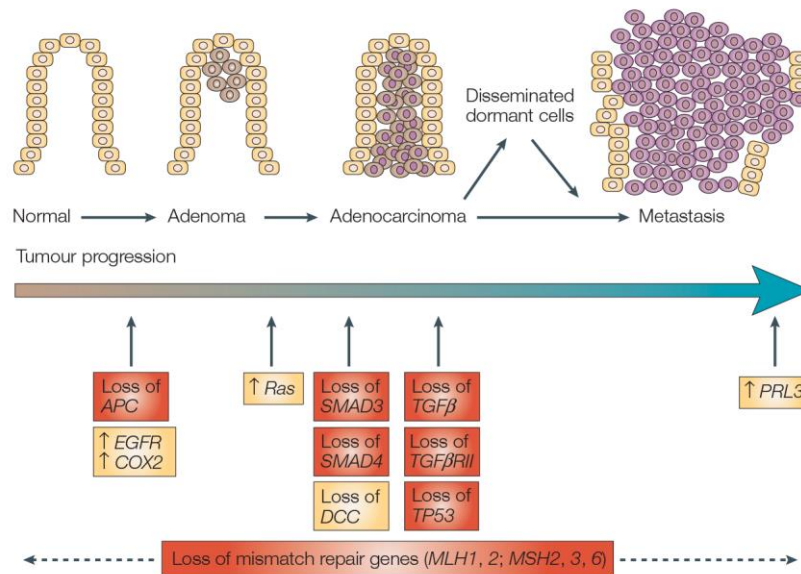
Figure 1.

The mutations occurring during multi-step progression in colon cancer. The top half represents progressive lesion formation with altered cellular properties. The bottom half shows key genes deregulated during colorectal cancer progression.

(Figure taken from: Green JE, *et al. Nature Reviews Cancer*, 2005) [7]

1.2 Colorectal cancer

Among all different types of cancer, CRC is one of the leading causes of cancer death (Figure 2). In the United States alone 135,430 new cases and 50,260 deaths from CRC are expected in 2017 [8]. CRC is a multistep process driven by mutational activation of several oncogenes and genetic/epigenetic inactivation of tumor suppressors [9] (Figure 1). The majority of CRCs originate from benign adenomas, which are caused by inactivating mutations in the *adenomatous polyposis coli (APC)* gene [10]. *APC* mutation leads to the constitutive activation of the Wnt/β-catenin pathway which results in the increased expression of β-catenin [11], a critical regulator of intestinal epithelial cell homeostasis [12]. During CRC progression

additional mutations in key oncogenes and tumor suppressor genes, such as

p53 [4,13], are acquired.
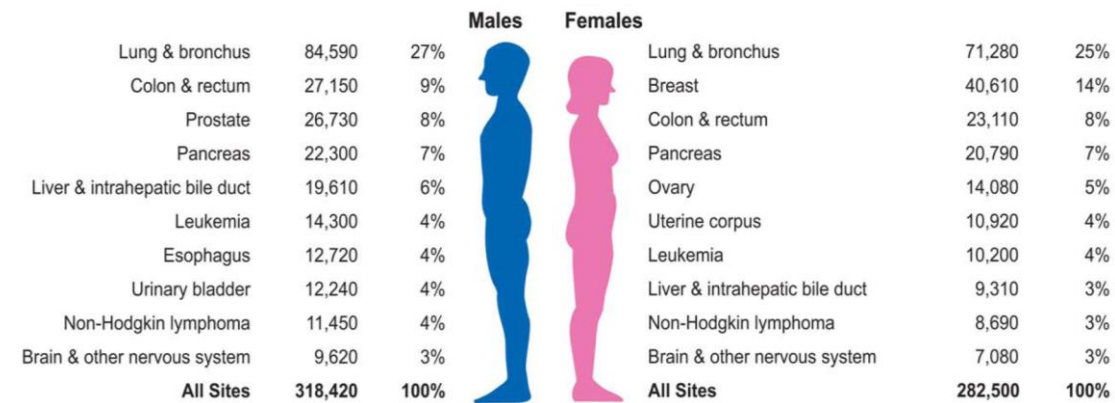
Figure 2.
Ten leading estimated cancer deaths by sex, United States, 2017. Estimates are rounded to the nearest 10 and cases exclude basal cell and squamous cell skin cancers and in situ carcinoma except urinary bladder.
(Figure taken from: Siegel RL, *et al. CA: A Cancer Journal For Clinicians*, 2017) [8]

1.3 The p53 tumor suppressor

The tumor suppressor protein p53 is a central regulator of the stress response and plays a crucial role in suppression of tumorigenesis [14]. p53 is induced by acute DNA damage or other cellular stresses that result in DNA damage, such as replication stress caused by oncogene activation. Activated p53 promotes cell cycle arrest, apoptosis and senescence (Figure 3). These effects of p53 activation contribute to the elimination of damaged cells, which would otherwise progress to tumors, thereby mediating suppression of tumorigenesis. p53 is inactivated in ca. 60% of CRCs [15]. Mutations in *p53* often increase the aggressiveness and malignancy of tumors and are

associated with poor patient prognosis. Although the p53 tumor suppressor has been extensively studied in the past 25 years, it is still unclear which and how its downstream targets mediate tumor suppression. Besides regulating the expression of mRNAs, p53 also controls the expression of non-coding RNAs, such as lncRNAs and microRNAs (miRNAs) [16,17], not only at the transcriptional level but also at the steps of processing and maturation [18]. Many tumor suppressive functions of p53 are thought to be mediated by p53-induced miRNAs [19,16]. Among the p53-induced microRNA-encoding genes, *miR-34a* and *miR-34b/c* display the most consistent and pronounced induction after p53 activation which may explain why they were identified as one of the first p53-regulated miRNAs [20,21].
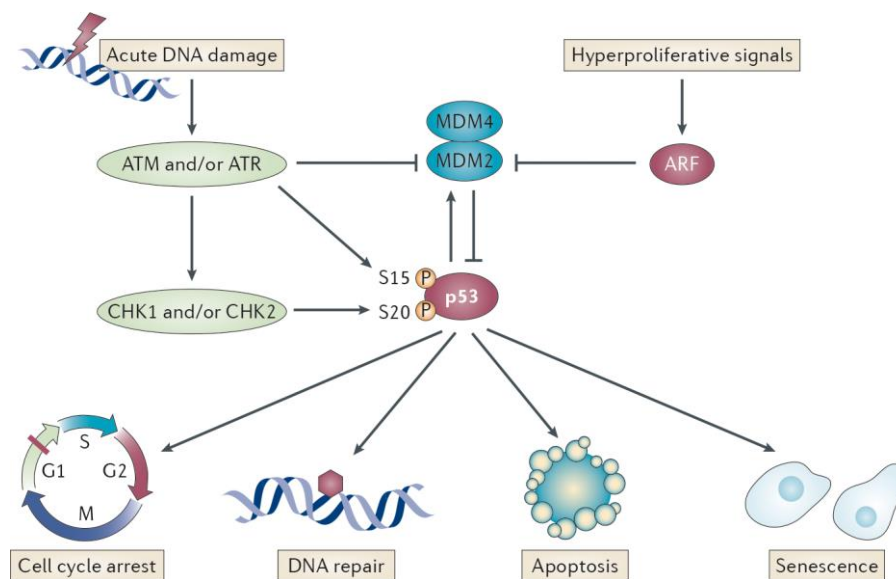
Figure 3.

The classical view of p53 activation and response. In response to acute DNA damage signals and hyper-proliferative signals are the most well established molecular models for p53 activation.

(Figure taken from: Bieging KT, *et al. Nature Reviews Cancer*, 2014) [22]

1.4 The miR-34 family

miRNAs are a class of non-protein coding RNAs and with a length of ~22 nucleotides. They play important roles in regulating their target mRNAs. The nucleotide positions 2 – 8 of the miRNA are called "seed region" and are partially complementary to a site in 3'-UTR of its target mRNAs, the so-called "seed-matching region". The mature miRNA and associated proteins form a RNA-induced silencing complex (miRISC). After association with the seed-matching region, miRNAs either lead to cleavage or to translational suppression of the respective target mRNAs (Figure 4) [23].

Among all miRNAs, miR-34a and miR-34b/c show the most marked induction by p53. The *miR-34a* gene is located on chromosome 1p36.22 and *miR-34b/c* genes are located on 11q23.1. The promoters of *miR-34a* and *miR-34b/c* contain several p53 responsive elements and p53 can directly bind to these elements and induce transcription. *miR-34*a and *miR-34b/c* presumably mediate tumor suppression by p53 via down-regulation of key-regulators numerous cancer associated processes, such as cell proliferation and survival [20], EMT [24], metastasis [25] and stemness [26] (Figure 5). Interestingly, some of these targets form feedback loops with p53 and miR-34s to regulate p53 functions [19]. For example, the oncogenic transcription factor c-Myc, which induces cell growth and proliferation, is directly repressed by miR-34a/b/c [27]. By repression of Sirt1, a deacetylase negatively regulating p53, miR-34a induces senescence [28]. Raver-Shapira *et al.* found that inhibition of miR-34a protects cells from this effect in wild-type p53 cells which suggests that miR-34a is, at least in part, required for p53-induced apoptosis [21].

Cancer stem cells (CSCs) account for cancer initiation, progression, and recurrence [29]. miR-34 levels are reduced in the CSC population of cancer cell lines [30,31] and re-expression of miR-34 in cancer cells can block tumor regeneration and metastasis [32]. miR-34a/b/c presumably function as cell-fate determinants in colonic cancer stem cells (CCSC) by regulating Notch activity as it directly targets the *Notch1* and *Numb* mRNAs [33,34]. Furthermore, miR-34a/b/c regulate the homeostasis of normal stem cells [35] and suppress the formation of induced pluripotent stem cells (IPSCs) [36].

Consistent with a tumor suppressive role in tumorigenesis, down-regulation of *miR-34a/b/c* expression has been observed in a variety of human cancers [16]. *miR-34a/b/c* expression was reported to be down-regulated in CRC cell lines due to epigenetically silencing by CpG methylation [37]. In primary CRCs, 74% *miR-34a* and 99% *miR-34b/c* were methylated [38,39]. These findings suggest important roles of *miR-34a/b/c* as downstream effectors of p53 and potential tumor suppressors of CRC. In line with its tumor suppressive potential miR-34a mimetics are currently tested in the clinics for treatment of advanced cancer [40].

In mice, *miR-34a* is universally expressed and exhibits the highest levels of expression in the brain [41]. *miR-34b/c* is mainly expressed in the lung and almost undetectable in other tissues [41]. Surprisingly, opposed to *p53*-deficient mice, *miR-34a/b/c*-deficient mice did not show spontaneous tumorigenesis [42]. However, *miR-34a* deficiency stimulated tumorigenesis when one allele of *p53* was lost [43]. Besides, prostate epithelium specific inactivation of *miR-34a/b/c* and *p53* resulted in an enlarged prostate stem cell compartment and the development of invasive adenocarcinomas and high

8

grade prostatic intraepithelial neoplasia [35]. Taken together, these findings indicate that the miR-34 family may have tumor-suppressor function by regulating aspects of stem cell biology. Additionally, the double knockout of both *miR-34b/c* and *miR-449a/b/c,* another member of the miR-34 family*,* resulted in oligo-astheno-teratozoospermia and infertility in mice [44]. Furthermore, deletion of *miR-34a/b/c* and *miR-449a/b/c* alleles results in postnatal mortality, infertility and respiratory dysfunction due to a defective motile ciliogenesis, which was, at least in part, mediated by de-repression of Cp110, a centriolar protein suppressing cilia assembly [45].
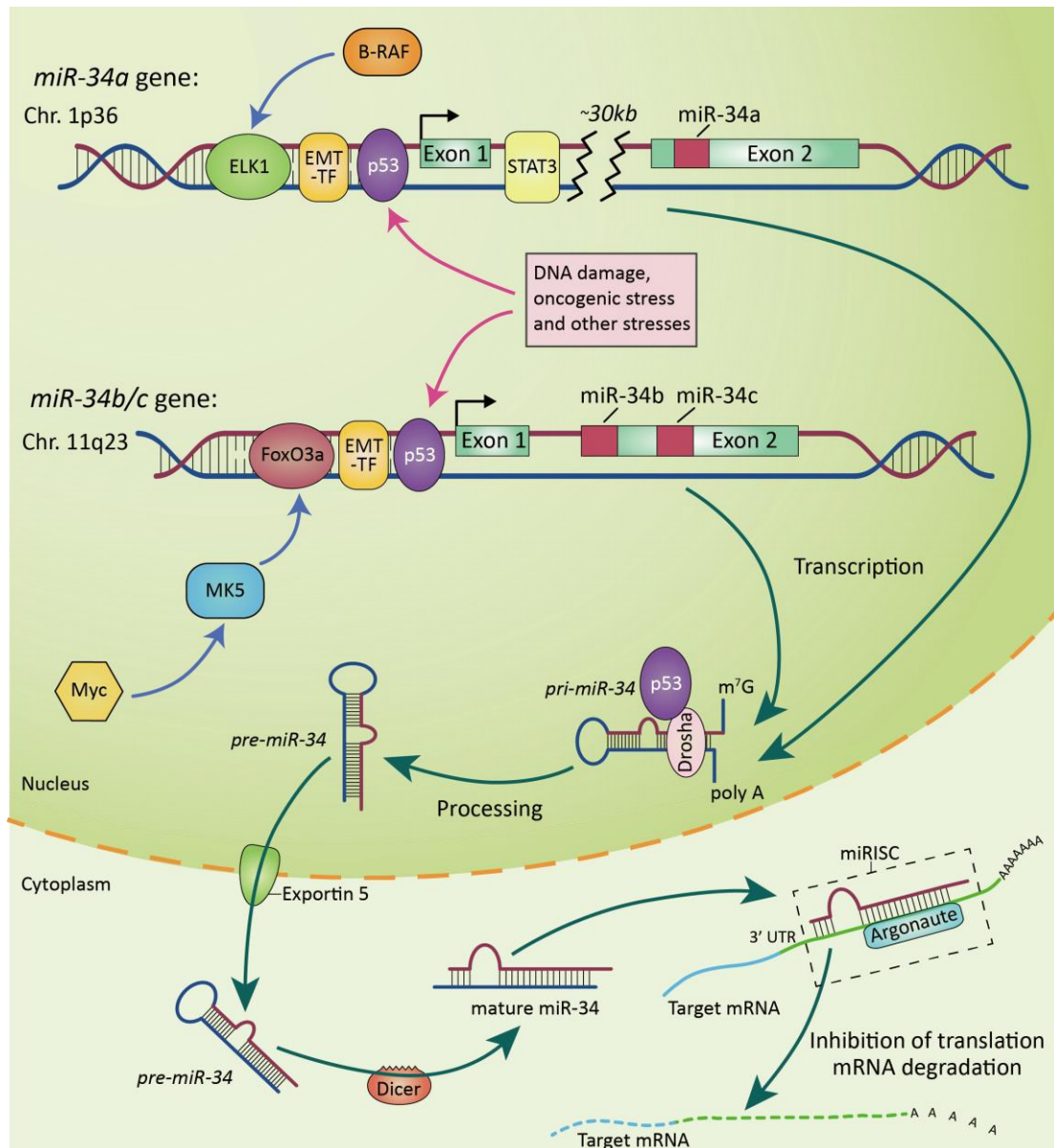
Figure 4.

Genomic structure and regulation of miR-34 family members. Structure of *miR-34a* and *miR-34b/c* genomic loci. Green and red boxes represent exons and miRNA hairpins, respectively.

(Figure taken from: Rokavec M, *et al*. *Journal of Molecular Cell Biology*, 2014) [19]
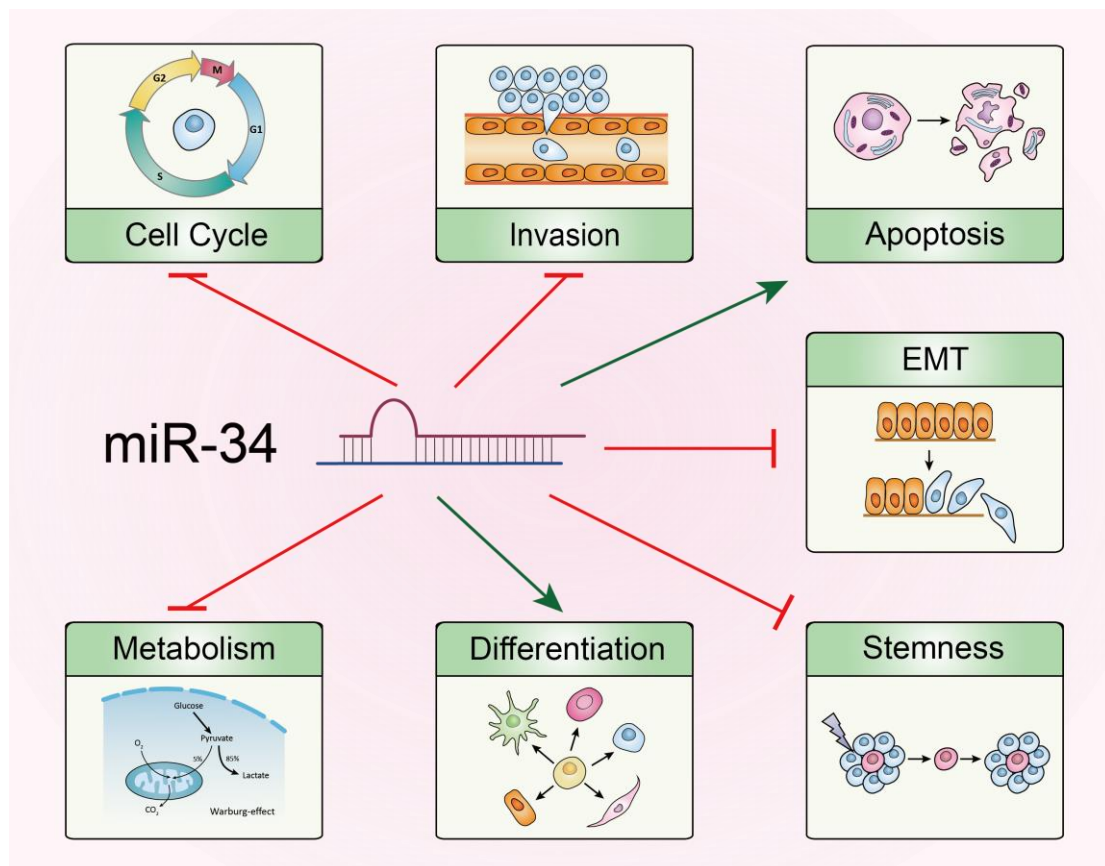
Figure 5.

miR-34 regulates cancer-relevant pathways. The net effect of regulation by miR-34 on each pathway/process is indicated by a green arrow (activation) or a red inhibitory symbol.
(Figure modified from: Rokavec M, *et al. Journal of Molecular Cell Biology*, 2014) [19]

1.5 The Wnt signaling pathway in colorectal cancer

Wnt signaling is one of the essential pathways involved in embryonic development and stemness [46], and has been extensively studied and directly associated with tumorigenesis. The canonical WNT pathway is also known as WNT/β-catenin signaling. In the absence of WNT ligand, β-catenin is phosphorylated and degraded through a multi-protein complex consisting of the tumor-suppressor protein APC and glycogen synthase kinase 3β (GSK3β) [47]. When WNT ligands bind to Frizzled and LRP receptors at the cell

membrane and activate intracellular signaling, the phosphorylation and degradation of β-catenin is inhibited resulting in the nuclear translocation of β-catenin. In the nucleus, β-catenin binds to the TCF/LEF complex and induces the transcription of WNT target genes [48] (Figure 6).

The mechanisms of Wnt signaling in CRC cells are well studied and several related mouse models have been established, for example the $Apc^{Min/+}$ mice [49]. $Apc^{Min/+}$ mice inherit a mutant Apc allele, that results in a truncation of the APC protein at amino acid 850 [50], and spontaneously lose the wild-type Apc allele causing multiple benign adenomas mainly throughout the small intestine [51]. In humans, inherited germ-line mutations in one APC allele will lead to hundreds to thousands of adenomatous polyps mainly in the colon and rectum by the age of 25. The syndrome is known as familial adenomatous polyposis (FAP). Because of the large number of polyps, the patients will almost certainly develop CRCs in their forties to fifties [52,9]. To prevent the formation of CRCs part or all of their colon is surgical removed. As the early loss of APC is a hallmark of inherited and almost all sporadic CRCs, $Apc^{Min/+}$ mice allow to study the influence of putative tumor suppressor genes on the initiation of intestinal tumorigenesis [53].

Furthermore, β-catenin, the critical mediator of colon carcinogenesis [12] is a miR-34 direct target [54]. In our previous study, decreased $miR-34a$ and increased β-catenin expression are associated with liver metastases of CRC [39]. Therefore, we generated mice $Apc^{Min/+}$ mice carrying deletions of $miR-34a$ and miR-34b/c to determine their role in intestinal tumorigenesis.
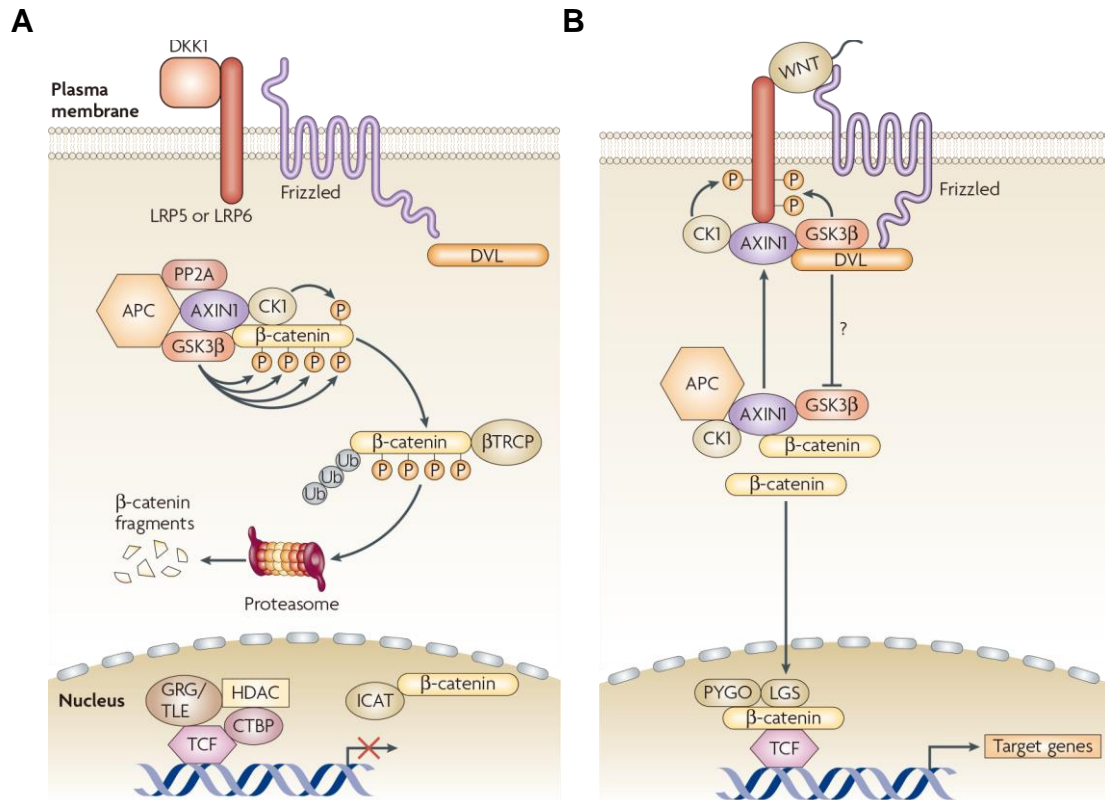
Figure 6.

Canonical WNT-β-catenin signaling.

A. In the absence of WNT ligands, β-catenin is phosphorylated and degraded. The level of nuclear β-catenin is low.

B. When WNT ligands bind to the receptor, β-catenin translocates to the nucleus and induces the transcription of WNT target genes.

(Figure taken from: Staal FJ, *et al. Nature Reviews Immunology*, 2008) [55]

2. Aims of the study

The present work had the following aims:

1) Characterization of the biological function of *miR-34a/b/c* in the intestine using mice with deletions of their host genes.

2) Evaluation of the tumor suppressive function of *miR-34a/b*/c in multiple intestinal neoplasia (*Apc*^{Min/+}) mice.

3) Comprehensive analysis of the effector network of *miR-34a/b/c* in intestinal adenoma development.

14

3. Materials

3.1 Chemicals and reagents

Chemical compound	Supplier
Ampicillin	Sigma-Aldrich Co. LLC., USA
Antibody Diluent with Background-Reducing Components	Agilent Technologies, USA
APS (ammonium peroxodisulfate)	Carl Roth GmbH + Co. KG, Germany
B-27® Supplement (50X), minus vitamin A	Thermo Fisher Scientific Inc., USA
BD Matrigel™ Basement Membrane Matrix	BD Bioscience, Germany
Blocking Reagent	Roche Diagnostics GmbH, Germany
CHAPS (3-[(3-Cholamidopropyl)dimethyl ammonio]-1-propane sulphonate)	Sigma-Aldrich Co. LLC., USA
cOmplete Mini Protease Inhibitor Cocktail Tablets	Roche Diagnostics GmbH, Germany
DAPI (4',6-diamidino-2-phenylindole)	Carl Roth GmbH + Co. KG, Germany
Diethyl pyrocarbonate	Sigma-Aldrich Co. LLC., USA
Distilled Water	Thermo Fisher Scientific Inc., USA
DMEM (Dulbecco's Modified Eagle Medium)	Thermo Fisher Scientific Inc., USA
DMSO (dimethyl-sulfoxide)	Carl Roth GmbH + Co. KG, Germany
dNTPs (deoxynucleotides triphosphate)	Thermo Fisher Scientific Inc., USA
Doxycycline hyclate	Sigma-Aldrich Co. LLC., USA
EGF Recombinant Mouse Protein	Thermo Fisher Scientific Inc., USA
Ethidium bromide	Carl Roth GmbH + Co. KG, Germany
Fast SYBR® Green Master Mix	Thermo Fisher Scientific Inc., USA
FBS (fetal bovine serum)	Thermo Fisher Scientific Inc., USA
Formamide	Sigma-Aldrich Co. LLC., USA
FuGENE® 6 Transfection Reagent	Promega GmbH, Germany

Chemical compound	Supplier
Gene Ruler 100bp plus DNA ladder	Thermo Fisher Scientific Inc., USA
Gene Ruler Low Range DNA ladder	Thermo Fisher Scientific Inc., USA
GlutaMAX™ Supplement	Thermo Fisher Scientific Inc., USA
HBSS (Hank's Balanced Salt Solution)	Thermo Fisher Scientific Inc., USA
Heparin sodium	Sigma-Aldrich Co. LLC., USA
Hi-Di™ Formamide	Thermo Fisher Scientific Inc., USA
HiPerFect Transfection Reagent	Qiagen GmbH, Germany
Immobilon Western HRP Substrate	Merck Millipore, Germany
Immobilon®-P PVDF Membrane	Merck Millipore, Germany
LB agar (Lennox)	Carl Roth GmbH + Co. KG, Germany
LB medium (Luria/Miller)	Carl Roth GmbH + Co. KG, Germany
Methanol	Carl Roth GmbH + Co. KG, Germany
NaCl	Carl Roth GmbH + Co. KG, Germany
O'Gene Ruler 1kb DNA ladder	Thermo Fisher Scientific Inc., USA
Opti-MEM™ Reduced Serum Media	Thermo Fisher Scientific Inc., USA
PageRuler™ Prestained Protein Ladder	Thermo Fisher Scientific Inc., USA
Paraformaldehyde	Merck Millipore, Germany
Penicillin-Streptomycin	Thermo Fisher Scientific Inc., USA
peqGOLD Universal-Agarose	VWR Peqlab, Germany
POP-6™ Polymer for 3130/3130xl Genetic Analyzers	Thermo Fisher Scientific Inc., USA
ProLong® Gold antifade reagent	Thermo Fisher Scientific Inc., USA
RNA from yeast	Roche Diagnostics GmbH, Germany
Rotiphorese gel 30 (37,5:1)	Carl Roth GmbH + Co. KG, Germany
SDS (sodium dodecyl sulfate)	Carl Roth GmbH + Co. KG, Germany
Sigma-Aldrich Co. LLC.,	Sigma-Aldrich Co. LLC., USA
Skim milk powder	Sigma-Aldrich Co. LLC., USA
Sodium citrate dihydrate	Sigma-Aldrich Co. LLC., USA

Chemical compound	Supplier
Target Retrieval Solution, Citrate pH 6	Agilent Technologies, USA
Temed (N,N,N',N'-Tetramethylethylenediamine, 1,2-Bis(dimethylamino)-ethane)	Carl Roth GmbH + Co. KG, Germany
Tris-base	Carl Roth GmbH + Co. KG, Germany
Triton® X 100	Carl Roth GmbH + Co. KG, Germany
Tween® 20	Sigma-Aldrich Co. LLC., USA

3.2 Enzymes

Enzyme	Supplier
Collagenase Type IV	Biochrom GmbH, Germany
Dispase II	Sigma-Aldrich Co. LLC., USA
DNase I (RNase-Free)	New England BioLabs GmbH, Germany
HOT FIREPol® DNA Polymerase	Solis BioDyne, Estonia
Pfu DNA Polymerase	Thermo Fisher Scientific Inc., USA
Proteinase K	Sigma-Aldrich Co. LLC., USA
Restriction Endonuclease	New England BioLabs GmbH, Germany
T4 DNA Ligase	Thermo Fisher Scientific Inc., USA
Trypsin (10x)	Thermo Fisher Scientific Inc., USA

3.3 Kits

Kit	Supplier
BCIP®/NBT Liquid Substrate System	Sigma-Aldrich Co. LLC., USA
BigDye® Terminator v1.1 Cycle Sequencing Kit	Thermo Fisher Scientific Inc., USA
DAB Substrate Kit	Vector Laboratories, Inc., USA
DIG Northern Starter Kit	Roche Diagnostics GmbH, Germany
Dual-Luciferase® Reporter 1000 Assay Systems	Promega GmbH, Germany
DyeEx 2.0 Spin Kit	Qiagen GmbH, Germany
High Pure RNA Isolation Kit	Roche Diagnostics GmbH, Germany
ImmPRESS™ HRP Anti-Goat IgG (Peroxidase) Polymer Detection Kit	Vector Laboratories, Inc., USA
ImmPRESS™ HRP Anti-Rabbit IgG (Peroxidase) Polymer Detection Kit	Vector Laboratories, Inc., USA
Micro BCA™ Protein Assay Kit	Thermo Fisher Scientific Inc., USA
PureYield™ Plasmid Midiprep System	Promega GmbH, Germany
QIAprep Spin Miniprep Kit	Qiagen GmbH, Germany
QIAquick Gel Extraction Kit	Qiagen GmbH, Germany

Kit	Supplier
QIAquick PCR Purification Kit	Qiagen GmbH, Germany
RNeasy Plus Mini Kit	Qiagen GmbH, Germany
VECTASTAIN Elite ABC HRP Kit	Vector Laboratories, Inc., USA
Verso cDNA Synthesis Kit	Thermo Fisher Scientific Inc., USA

3.4 Antibodies

3.4.1 Primary antibodies

Name	Species	Catalog No.	Company	Use	Dilution	Source
Lysozyme	Mouse	LS-C138144	LSBio	IHC	1:1000	Rabbit
β-catenin	Mouse	ab32572	Abcam	IHC	1:500	Rabbit
Ki-67	Mouse	#12202	CST	IHC	1:400	Rabbit
Cleaved-Caspase-3	Mouse	#9664	CST	IHC	1:500	Rabbit
WASF1	Human Mouse	ab185546	Abcam	WB	1:5000	Rabbit
β-actin	Human Mouse	A2066	Sigma-Aldrich	WB	1:1000	Rabbit
Vimentin	Mouse	sc-7557	Santa Cruz	IHC	1:100	Goat
F4/80	Mouse	MF48000	Invitrogen	IHC	1:200	Rat
CD45R	Mouse	550286	BD	IHC	1:100	Rat
CD3	Mouse	A 0452	DAKO	IHC	1:100	Rabbit
MUC1	Mouse	ab15481	Abcam	IHC	1:100	Rabbit

IHC: Immunohistochemistry, WB: Western blot analysis

3.4.2 Secondary antibodies

Name	Species	Catalog No.	Company	Use	Dilution	Source
Anti-Rabbit IgG-Peroxidase	Rabbit	A0545	Sigma-Aldrich	WB	1:10000	Goat
Biotinylated Rabbit Anti-Rat Immunoglobulins	Rat	E 0468	DAKO	IHC	1:300	Rabbit

Name	Species	Catalog No.	Company	Use	Dilution	Source
Biotinylated Goat Anti-Rabbit Immunoglobulins	Rabbit	E 0432	DAKO	IHC	1:500	Goat

IHC: Immunohistochemistry, WB: Western blot analysis

3.5 Vectors and oligonucleotides

3.5.1 Vectors

Name	Insert	Source
pRTR-*pri-miR-34a*	human *pri-miR-34a*	[56]
pGL3-control-MCS	firefly luciferase	Promega GmbH, Germany
pGL3-*Wasf1*	mouse *Wasf1* 3'UTR	this work
pRL	*Renilla* luciferase	Promega GmbH, Germany
pBluescript II SK(+)-mOLMF4	mouse *Olfm4*	Dr. Hans Clevers

3.5.2 Oligonucleotides

3.5.2.1 Oligonucleotides used for genotyping

Name	Sequence (5' - 3')	Product
miR_34a-Fwd	ACCTTGCAGGTGCTCAGAAT	Floxed 368bp
miR_34a-Rev-2	TGGAGCTAACGGAGTGTGTG	Wildtype 510bp
miR_34a-Rev-4	CTACCCAAGCTCGACGAAGT	Knockout 623bp
miR_34a-Rev-8	TGCAGCACTTCTAGGGCAGT	
miR_34bc-A	CTGCGCTTCTTTCTTCGATGTAGC	Wildtype 177bp
miR_34bc-B	TGGCTTTAGGATCTCCATTTCAGC	Knockout 244bp
miR_34bc-D	ACCTGGTTAAGTGGGCTGAGTTCC	Floxed 335bp
APCmin-Mut	TTCTGAGAAAGACAGAAGTTA	Mutation 340bp
APCmin-Common	TTCCACTTTGGCATAAGGC	Wildtype 600bp

Name	Sequence (5' - 3')	Product
APCmin-Wt	GCCATCCCTTCACGTTAG	

3.5.2.2 Oligonucleotides used for cloning

Name	Use	Sequence (5' - 3')
Mmu-c-AgeI-Wasf1-For	Cloning 3'-UTR	TGAACCGGTAACACGAGC GGATTGAAAAC
Mmu-c-PstI-Wasf1-Rev		AAACTGCAGGGAAGGGG TTCTGCTAAACG
Wasf1-clone-seq-F1	Sequencing Insert	TATTGCAAGGCTGAATGC AC
Wasf1-clone-seq-R1		TCCAGGGGGAAAAATTAA GG

3.5.2.3 Oligonucleotides used for qPCR

Name	Sequence (5' - 3')
Mmu-q-Axl-For	CTATCCAGGGGTGGAGAACA
Mmu-q-Axl-Rev	ACCGAGACATCAGGGCATAC
Mmu-q-Pdgfra-For	ACAGAGACTGAGCGCTGACA
Mmu-q-Pdgfra-Rev	ACTGGAACCTGTCTCGATGG
Mmu-q-Pdgfrb-For	AACCCCCTTACAGCTGTCCT
Mmu-q-Pdgfrb-Rev	TTGCCTTCTCTGCCACTCTT
Mmu-q-Igf1-For	TGGATGCTCTTCAGTTCGTG
Mmu-q-Igf1-Rev	GCAACACTCATCCACAATGC
Mmu-q-Inhbb-For	TCCGAGATCATCAGCTTTGCA
Mmu-q-Inhbb-Rev	TCTCCAGGACATAGGGGAGC
Mmu-q-Wasf1-For	CCACCCTGCCTGTAATCAGT
Mmu-q-Wasf1-Rev	GTTTTCAATCCGCTCGTGTT
Mmu-q-Stc1-For	ACAGCTGCCCAATCACTTCT
Mmu-q-Stc1-Rev	TCTCCATCAGGCTGTCTCTG
Mmu-q-Fgfr1-For	TTACCCAGTTGGGTCTGTCC
Mmu-q-Fgfr1-Rev	TTCTGTTTCCTGAGGGATGG
Mmu-q-Actin-For	CTAAGGCCAACCGTGAAAAG
Mmu-q-Actin-Rev	ACCAGAGGCATACAGGGACA

Name	Sequence (5' - 3')
Mmu-q-Col4a2-For	GTGCACAGCCAGGATACCTC
Mmu-q-Col4a2-Rev	CCCCCGTTACACTCGATAAA
Mmu-q-Col6a2-For	GCCTTCCCACTGACCTACAA
Mmu-q-Col6a2-Rev	TTGTTGATGGCGTGTACGAT
Mmu-q-Cacna2d2-For	GCCCCTAGTAGGACCACACA
Mmu-q-Cacna2d2-Rev	AGCCAGGAGAGACCAACTCA
Mmu-q-Ctnnb1-For	AGGGTGGGAATGGTTTTAGG
Mmu-q-Ctnnb1-Rev	GTGGCAAAAACATCAACGTG
Mmu-q-Lef1-For	ACAGGTCCCAGAATGACAGC
Mmu-q-Lef1-Rev	TGGAGACAGTCTGGGGTTTC
Mmu-q-Lrp6-For	TGATCGGAGAGGGTATGAGG
Mmu-q-Lrp6-Rev	AAGAACTCTTGGGCCTTGGT
Mmu-q-Zeb1-For	GCATGTGACCTGTGTGACAA
Mmu-q-Zeb1-Rev	GATAGGGCTTTTCCCCAGAG
Mmu-q-Twist1-For	CCCACCCCACTTTTTGACGA
Mmu-q-Twist1-Rev	GGGATGCCTTTCCTGTCAGT
Mmu-q-Fn1-For	AGTGCTTCATGCCGCTAGAT
Mmu-q-Fn1-Rev	GGGTGAAAGGACCACTCAAA
Mmu-q-Ccnd1-For	GCGTACCCTGACACCAATCTC
Mmu-q-Ccnd1-Rev	CTCCTCTTCGCACTTCTGCTC
Mmu-q-Wnt1-For	GCGTTCTGCACGAGTGTCTA
Mmu-q-Wnt1-Rev	GGTAGGGTGGGCAAACATCA
Mmu-q-Wnt3-For	CGGCTTTACAGAGGGGCTTT
Mmu-q-Wnt3-Rev	TAGCCCAGCCTGTTCTGTTG
Mmu-q-Muc1-For	GACATCTTTCCAACCCAGGA
Mmu-q-Muc1-Rev	GGGGTGACTTGCTCCTACAA
Mmu-q-Tff3-For	AATGTGCCCTGGTGCTTCAA
Mmu-q-Tff3-Rev	GATCGGGGATGCTTGCTACC
Mmu-q-Retnlb-For	CTGATAGTCCCAGGGAACGC
Mmu-q-Retnlb-Rev	GTCTGCCAGAAGACGTGACA
Hsa-q-Wasf1-For	TGATGCCAGGAGTGTGCTAC
Hsa-q-Wasf1-Rev	GCGTTCATGCTTAGCTTCCT
Hsa-q-Actin-For	TGACATTAAGGAGAAGCTGTGCTA
Hsa-q-Actin-Rev	GAGTTGAAGGTAGTTTCGTGGATG

3.5.2.4 Oligonucleotides used for fluorescence *in situ* hybridization (FISH)

Name	Sequence (5' - 3')
universal eubacteria probe (EUB338) [57]	[FITC]-5'-GCTGCCTCCCGTAGGAGT-3'
negative control probe (NON338) [57]	[Cy3]-5'-CGACGGAGGGCATCCTCA-3'

3.5.3 miRNA mimics

miRNA mimics	Supplier
Pre-miR™ miRNA Precursor Negative Controls	Thermo Fisher Scientific Inc., USA
Pre-miR™ miRNA Precursor PM11030 (hsa-miR-34a-5p)	Thermo Fisher Scientific Inc., USA
Pre-miR™ miRNA Precursor PM11039 (hsa-miR-34c-5p)	Thermo Fisher Scientific Inc., USA

3.6 Buffers and solutions

3.6.1 Buffers for animal genotyping

Proteinase K buffer:

- 0.1 M Tris (pH 8.5)

- 0.2 M NaCl

- 5 mM EDTA (pH 8.0)

- 0.2% SDS

„Vogelstein" PCR buffer (10X) [58]:

- 166 mM NH_4SO_4

- 670 mM Tris (pH 8.8)

- 67 mM $MgCl_2$

- 100 mM β-mercapto-ethanol

3.6.2 Buffers and media for cell and tumor organoid culture

Cell culture medium:

- 90% DMEM medium

- 10% FBS

- 100 U/ml penicillin

- 100 µg/ml streptomycin

Cell freezing medium:

- 40% DMEM medium

- 50% FBS

- 10% DMSO

EDTA chelation buffer [59]:

- 2 mM EDTA

- 5.6 mM Na_2HPO_4

- 8.0 mM KH_2PO_4

- 96.2 mM NaCl

- 1.6 mM KCl

- 43.4 mM sucrose

- 54.9 mM D-sorbitol

- 0.5 mM DL-dithiothreitol

Adenoma cell digestion buffer [60]:

- 2.5% FBS

- 100 U/ml penicillin

- 100 µg/ml streptomycin

- 200 U/ml Type IV collagenase

- 125 µg/ml Type II dispase

- in DMEM medium

Tumor organoid culture medium [59]:

- 100 U/ml penicillin

- 100 µg/ml streptomycin

- 10 mmol/L HEPES

- 2 mM Glutamax

- 1x B27 supplement

- 50 ng/ml EGF

- in Advanced DMEM/F12

3.6.3 Buffers and solutions for Western blot analysis

RIPA buffer:

- 1% NP40

- 0.5% Sodium deoxycholate

- 0.1% SDS

- 150 mM NaCl

- 50 mM TrisHCl (pH 8.0)

Laemmli buffer (2X):

- 125 mM TrisHCl (pH 6.8)

- 4% SDS

- 20% glycerol

- 0.05% bromophenol blue

- 10% β-mercapto-ethanol

Electrode buffer (Tris/glycine/SDS running buffer) (10X):

- 144.0 g glycine

- 30.3 g Tris base

- 10.0 g SDS

- H_2O to 1000 ml

Transfer buffer:

- 200 mM glycine

- 20% methanol

- 25 mM Tris base (pH 8.6)

TBST (10X):

- 0.2 M Tris base

- 1.5 M NaCl

- 0.5% Tween 20

3.6.4 Buffers and solutions for *in situ* hybridization

PBS (10X):

- 1.37 M NaCl

- 27 mM KCl

- 100 mM Na_2HPO_4

- 18 mM KH_2PO_4

- Adjust pH to 7.2 wih HCl

SSC (5X):

- 0.75 M NaCl

- 0.075 M Sodium citrate

Tris/NaCl buffer

- 0.1 M TrisCl (pH 7.5)

- 0.15 M NaCl

- 0.1% Tween 20

Blocking solution:

- 1% blocking powder

- 1X Tris/NaCl buffer

Hybridization buffer:

- 50% formamide

- 5X SSC

- 2% blocking powder

- 0.05% CHAPS

- 5 mM EDTA

- 50 µg/ml heparin

- 1 µg/ml yeast RNA

NTM buffer:

- 0.1 M TrisHCl (pH 9.5)

- 0.1 M NaCl

- 0.05 M $MgCl_2$

3.6.5 Buffers and solutions for Fluorescence *in situ* hybridization

Hybridization buffer [61]:

- 0.9 M NaCl

- 20 mM Tris/HCl pH7.3

- 0.01% SDS

3.7 Animals

Strain	Background	Source
miR-34a^{fl/fl} mice	C57BL6/SV129	This work [62]
miR-34b/c^{fl/fl} mice	C57BL6/SV129	Dr. Alexander Nikitin (Cornell University) [35]
Flp mice	C57BL6	The Jackson Laboratory
CMV-Cre mice	C57BL6	The Jackson Laboratory
Apc^{Min/+} mice	C57BL6	Dr. Marlon Schneider (Ludwig-Maximilians-University of Munich)

3.8 Laboratory equipment

Device	Supplier
440CF Imaging System	Eastman Kodak Company, USA
Applied Biosystems® 3130 Genetic Analyzer	Thermo Fisher Scientific Inc.,USA
Applied Biosystems® GeneAmp PCR System 9700	Thermo Fisher Scientific Inc.,USA
AxioPlan 2 Microscope System	Carl Zeiss Meditec AG, Germany
Axiovert 25 Inverted Microscope	Carl Zeiss Meditec AG, Germany
Cell culture flasks, Multiwall plates and Conical Tubes	Corning Incorporated, USA
Eppendorf 5417C Centrifuge	Eppendorf GmbH, Germany
FluorChem FC2 Imaging System	ProteinSimple, USA
Forma™ Water-Jacketed CO2 Incubator	Thermo Fisher Scientific Inc.,USA
Hemacytometer	Thermo Fisher Scientific Inc.,USA
Heraeus™ Fresco™ Microcentrifuge	Thermo Fisher Scientific Inc.,USA
Heraeus™ Megafuge 1.0 Centrifuge	Thermo Fisher Scientific Inc.,USA
Heraeus™ Pico™ Microcentrifuge	Thermo Fisher Scientific Inc.,USA
Herasafe™ KS, Class II Biological Safety Cabinet	Thermo Fisher Scientific Inc.,USA
HTU SONI-130 MiniFIER Homogenizer	G. HEINEMANN Ultraschall- und Labortechnik, Germany
LightCycler® 480 Instrument II	Roche Molecular Systems Inc., USA

Device	Supplier
LSM 700 Laser Scanning Confocal Microscope	Carl Zeiss Meditec AG, Germany
Mastercycler™ pro PCR System	Eppendorf GmbH, Germany
Mini-PROTEAN® Electrophoresis System	Bio-Rad Laboratories, Inc., Germany
NanoDrop® ND-1000 Spectrophotometer	Thermo Fisher Scientific Inc.,USA
Orion II Microplate Lumimometer	Berthold Detection Systems GmbH, Germany
Varioskan™ Flash Multimode Reader	Thermo Fisher Scientific Inc.,USA
Waterbath WNB 45	Memmert GmbH + Co. KG, Germany

4. Methods

4.1 Propagation of bacteria

4.1.1 Inoculation and cultivation of bacteria

The *E.coli* XL1-blue strain was used for cloning and production of plasmids. The bacteria were propagated in liquid culture (LB-medium, shaking at 225 rpm) or on solid culture (LB-agar) at 37°C overnight. An ampicillin selection (100 µg/ml ampicillin) was used to select the bacteria carrying plasmids with ampicillin resistance gene. All vectors used in this work contained an ampicillin resistance cassette.

4.1.2 Transformation

One hundred microliter aliquot of *E.coli* XL1-blue cells were thawed on ice and then added 100 ng of plasmid DNA to the cells. After 30 minutes stand on ice, cells were incubated at 42°C for 60 seconds and put back on ice for 5 minutes. Then 900 µl LB-medium was added and cells were incubated at 37°C for 1 hour. To increase colony number, cells were centrifuged at 2000 rpm for 5 minutes and removed the supernatant. Finally, the remaining cells were resuspended and spread onto a pre-warmed (37°C) culture plate with LB-agar containing ampicillin at 37°C overnight.

4.1.3 Purification of plasmid DNA from bacteria

Bacterial cell was cultured in either 5 ml (small amount) or 150 ml (big amount) LB-medium with ampicillin overnight at 37°C (shaking at 225 rpm). For the small amount plasmid DNA isolation, QIAprep Spin Miniprep Kit (QIAGEN) was used according to the handbook from the manufacturer. For

the big amount plasmid preparation, PureYield Plasmid Midiprep System (Promega) was used by following the instruction of the manufacturer.

4.2 Mammalian cell culture

4.2.1 Propagation of mammalian cell lines

H1299 lung cancer cells used for 3'-UTR reporter assays were from own stocks and their negativity for p53 were validated. SW620 CRC cells used for ectopic *pri-miR-34a* expression were from own stocks and authenticated by STR analysis in 2014 (Eurofins Genomics, Ebersberg, Germany). H1299 and SW620 cancer cell lines were kept in Dulbecco's modified Eagle's medium (DMEM) with 10% fetal calf serum (Invitrogen), 100 U/ml penicillin and 100 μg/ml streptomycin at a 37°C and 5% CO_2 humid incubator. All cell lines were passaged every 3 days.

4.2.2 Transfection of plasmids

For the transfection of plasmid vectors, SW620 cells were trypsinized and seeded into a 12-well plate at 2×10^5 cells per well with 900 μl Opti-MEM medium. 3 μl FuGENE 6 transfection reagent (Promega) was diluted in 100 μl Opti-MEM medium and incubated at room temperature for 5 minutes. 2 μg of plasmid DNA was added to the FuGENE 6/medium, mixed immediately and incubated for 25 minutes. The transfection reagent mix was added to the cells drop-wise, and then returns cells to the incubator for 24 - 48 hours before assay.

4.2.3 Conditional expression in cell pools

SW620 cells were transfected with episomal pRTR-*pri-miR-34a* [24] expression plasmids. After 24 hours cell pools were selected by addition of Puromycin (2 µg/ml) for 10 days. GFP expression was evaluated by fluorescence microscopy 48 hours after addition of 100 ng/ml Doxycycline (DOX) to the cell pools.

4.2.4 Cryo-preservation of mammalian cells

Cells were trypsinized and resuspended in complete medium. After determination of the total number of cells, cell suspension was centrifuged at 200 g for 5 minutes. Supernatant was removed and the cells were resuspended in cold freezing medium. The cell suspension was then dispensed into cryogenic storage vials. The aliquots were placed in an isopropanol chamber and stored at -80°C overnight, then transferred to liquid nitrogen in the second day.

4.3 Generation of mice

4.3.1 Generation of *miR-34a/b/c-/-* mice

The generation of *miR-34a-/-* mice with a C57BL6/SV129 back-ground has been described previously [62]. *miR-34b/c*fl/fl mice were kindly provided by Dr. Alexander Nikitin (Cornell University, New York, USA) [35]. In brief, gene-specific deletions were generated by using homologous recombination with a vector containing *miR-34a* or *miR-34b/c* sequences flanked by *loxP* sites and an intronic Neomycin resistance (*Neo*) cassette flanked *frt* sites individually [62]. The *Neo* cassette was removed by crossing with *flp*-mice and germ-line

miR-34a or *miR-34b/c* knock-out mice were generated by crossing with *CMV-Cre* mice. *miR-34a/b/c⁻ᐟ⁻* compound mice were generated by crossing *miR-34a⁻ᐟ⁻* and *miR-34b/c⁻ᐟ⁻*.

4.3.2 Generation of *miR-34a/b/c⁻ᐟ⁻*; *Apc^Min/+* mice

miR-34a⁻ᐟ⁻, *miR-34b/c⁻ᐟ⁻*, *miR-34a⁻ᐟ⁻*; *miR-34b/c⁻ᐟ⁻* and *miR-34a⁺ᐟ⁺*; *miR-34bc⁺ᐟ⁺* mice were crossed with *Apc^Min/+* mice to obtain mice with the following genotypes: *miR-34a⁻ᐟ⁻*; *Apc^Min/+*, *miR-34b/c⁻ᐟ⁻*; *Apc^Min/+*, *miR-34a/b/c⁻ᐟ⁻*; *Apc^Min/+*, and *miR-34a/b/c⁺ᐟ⁺* *Apc^Min/+*. Mice were housed in individually ventilated cages (IVC). Animal studies were approved by the Government of Upper Bavaria, Germany (AZ 55.2-1-54-2532-4-2014).

4.4 Tumor organoid formation assay

4.4.1 Isolation of tumor cells from murine intestinal adenomas

Eighteen weeks old wild-type *Apc^Min/+* and *miR-34a/b/c⁻ᐟ⁻*; *Apc^Min/+* mice were sacrificed and intestine was collected and flushed with cold sterile PBS. Longitudinal opened intestinal fragments were incubated in EDTA chelation buffer on ice for 60 minutes. After incubation, the intestinal fragments were washed with cold chelation buffer two times and with cold sterile PBS two more times. Adenomas were then isolated from intestine and cut into 1 - 2 mm^3 fractions. Next, the adenoma fractions were incubated in adenoma cell digestion buffer for 2 hours at 37°C. Allow the adenoma fractions to settle down for 1 minute at normal gravity. The supernatant was collected in a 15 ml falcon tube, pelleted by centrifuging at 200 g for 5 minutes and washed once with cold sterile PBS.

4.4.2 Tumor organoid culture

Adenoma cells were resuspended in sterile PBS, and counted using a hemocytometer. Single adenoma cells were centrifuged at 200 g for 5 minutes, embedded in 4 mg/ml cold Matrigel on ice and seeded in 24-well plates at 15,000 cells per 50 µl Matrigel per well. The plates were then incubated at 37°C for 20 minutes until the Matrigel was fully polymerized and 500 µl tumor organoid culture medium containing 50 ng/ml mouse EGF was added per well. The plates were kept at a 37°C and 5% CO_2 humid incubator.

4.4.3 Cryo-preservation of tumor organoids

Medium was removed and 1 ml of ice-cold sterile PBS was added to each well, tumor organoids were disrupted by a P1000 sterile pipette with tips cut off and transferred to a 1.5 ml microcentrifuge tube. The supernatant was passed through a 27-gauge syringe 5 times, and then centrifuged 200 g for 5 minutes at 4°C. Resuspend the pellet in freezing medium, the tumor organoid suspension was then dispensed into cryogenic storage vials. The freezing containers were placed in an isopropanol chamber and stored at -80°C for 24 hours, then transferred to liquid nitrogen.

4.5 Isolation of DNA from mouse tails

Tail biopsies were obtained form 3 weeks old mice and placed to a 1.5 ml microcentrifuge tube. 300 µl Proteinase K buffer and 3 µl Proteinase K (10 mg/ml) were added to each tail sample tube. The microcentrifuge tubes were incubated at 55°C overnight and then heated at 95°C for 10 minutes to

inactivate the Proteinase K. After centrifugation at 13,000 g for 5 minutes, the supernatant which containing mouse DNA was directly used to perform the genotyping PCR.

4.6 PCR methods

4.6.1 Genotyping PCR

The genotyping PCR method for each gene was as followed:

*Apc*Min/+ genotyping:

Mastermix components (µl)		Thermocycling conditions		
Component	Vol.	Step	Temp	Time
Vogelstein PCR buffer (10X):	2.5	Initial	95°C	15 min
Tween 20	0.5	37 Cycles	95°C	30 sec
10 mM dNTPs	1.0		59°C	30 sec
10 µM Mut Primer	1.0		72°C	40 sec
10 µM Common Primer	1.0	Final	72°C	3 min
10 µM Wt Primer	0.5	Hold	4°C	
Hot Firepol *Taq* DNA Polymerase	0.5			
Nuclease-free water	16.0			
Genomic DNA	2.0			
Total	25.0			

miR-34a genotyping:

Mastermix components (µl)		Thermocycling conditions		
Component	Vol.	Step	Temp	Time
Vogelstein PCR buffer (10X):	2.5	Initial	95°C	15 min
Tween 20	0.5	37 Cycles	95°C	30 sec
10 mM dNTPs	1.0		65°C	30 sec
10 µM 34a-Fwd Primer	2.0		72°C	30 sec
10 µM 34a-Rev-2 Primer	1.0	Final	72°C	3 min
10 µM 34a-Rev-4 Primer	1.5	Hold	4°C	
10 µM 34a-Rev-8 Primer	0.5			
Hot Firepol *Taq* DNA Polymerase	0.5			

Nuclease-free water	13.5
Genomic DNA	2.0
Total	25.0

miR-34bc genotyping:

Mastermix components (µl)		Thermocycling conditions		
Component	Vol.	Step	Temp	Time
Vogelstein PCR buffer (10X):	2.0	Initial	95°C	15 min
Tween 20	0.5	37 Cycles	95°C	30 sec
10 mM dNTPs	0.5		59°C	30 sec
10 µM 34bc-A Primer	1.0		72°C	45 sec
10 µM 34bc-B Primer	1.0	Final	72°C	3 min
10 µM 34bc-D Primer	1.0	Hold	4°C	
Hot Firepol *Taq* DNA Polymerase	0.5			
Nuclease-free water	11.5			
Genomic DNA	2.0			
Total	20.0			

All genotyping primers are listed in chapter 3.5.2.1

4.6.2 Cloning of the *Wasf1* 3'-UTR

The 3'-UTR of *Wasf1* was PCR amplified from genomic DNA isolated form mouse tissue. The PCR product was inserted into pGL3-control-MCS vector (Promega) downstream of a firefly luciferase ORF, and verified by sequencing. All primers that were used for cloning are listed in chapter 3.5.2.2.

4.7 Isolation of RNA and reverse transcription

4.7.1 Isolation of RNA

High Pure RNA Isolation Kit (Roche) was used to isolate cultured mammalian cells. At least 1×10^6 cells were harvested for each sample, the cells were resuspended in PBS and followed the instruction of the

manufacturer. For the isolation of mice adenoma samples, a maximum amount of 20 mg fresh or frozen adenoma tissue was collected and added into Buffer RLT Plus (QIAGEN). Adenoma tissue was disrupted by a motorized homogenizer, and then the lysate was proceeded with RNeasy Plus Mini Kit (QIAGEN) with an on-column DNase I digestion according to the handbook from the manufacturer. The amount and quality of the isolated RNA was measured by NanoDrop spectrophotometer (Thermo Fisher Scientific).

4.7.2 Reverse transcription

Verso cDNA kit (Thermo Fisher Scientific) was used for cDNA synthesis according the instruction of the manufacturer.1 μg of total RNA and anchored Oligo-dT primer were used for reverse transcript reaction.

4.8 Quantitative real-time PCR (qPCR)

For analysis of mRNA expression levels, a LightCycler 480 Instrument II system (Roche) was used. qPCR reactions were conducted by using Fast SYBR Green Master Mix (Thermo Fisher Scientific). Relative gene expression was determined using the $2^{-\Delta\Delta Ct}$ method [63]. The individual mRNA levels were normalized to β-actin. All qPCR primers are listed in chapter 3.5.2.3.

4.9 Protein isolation and Western blot analysis

4.9.1 Protein isolation

4.9.1.1 Protein isolation from mammalian cells

Mammalian cells were cultured in general condition mentioned in chapter 4.2. Before harvest, cells were washed with cold PBS for two times, and then lysed in cold RIPA buffer with cOmplete Mini Protease Inhibitor (Roche) added. Lysates were sonicated and centrifuged at 16,000 g, 4°C for 15 minutes. The supernatant was collected to a new microcentrifuge tube and stored at -80°C for future use.

4.9.1.2 Protein isolation from murine adenomas

18 weeks old wild-type $Apc^{Min/+}$ and $miR\text{-}34a/b/c^{-/-}$; $Apc^{Min/+}$ mice were sacrificed and intestine was collected and flushed with cold sterile PBS. Adenomas were then isolated from intestine and cut into 1 - 2 mm^3 fractions. 10 volumes of cold RIPA buffer with protease inhibitor were added to the adenoma fractions, and then adenoma tissue was disrupted by a motorized homogenizer. Lysates were sonicated and centrifuged at 16,000 g, 4°C for 15 minutes. The supernatant was transferred to a new microcentrifuge tube and stored at a -80°C freezer.

4.9.2 Western blot analysis

4.9.2.1 Quantification of total protein

Micro BCA Protein Assay Kit (Thermo Fisher Scientific) was used to determine the protein concentration of the protein samples. Varioskan Flash

Multimode Reader (Thermo Fisher Scientific) was used to measure the absorbance of each sample and calculate the concentration.

4.9.2.2 Western blotting assay

30-60 µg whole lysate proteins were supplemented with 2X Laemmli buffer and heated at 99°C for 5 minutes to denature proteins. The protein lysates were then loaded onto a 7.5% - 12% SDS-polyacrylamide gel with PageRuler Prestained Protein Ladder (Thermo Fisher Scientific). Protein electrophoresis was performed by using Mini-PROTEAN Tetra Cell (Bio-Rad) at a voltage of 60 – 120 with electrode (running) buffer. Then the proteins were transferred to an Immobilon-P PVDF Membrane (Merck Millipore) by using Mini Trans-Blot Electrophoretic Transfer Cell (Bio-Rad) at 100 V, constant 350 mA with cold transfer buffer. Non-specific binding of the membrane was blocked by incubated in 5% skim milk/TBST buffer for 30 minutes. Then the membrane was transferred into TBST with primary antibodies diluted and incubated at 4°C overnight. Thereafter, the membrane was washed by TBST and incubated with secondary antibodies (HRP conjugated) at room temperature for 1 hour. For the detection, Immobilon Western HRP Substrate (ECL) (Merck Millipore) was applied to the membrane and 440CF Imaging System (KODAK) was used to detect chemiluminescent of the protein. All antibodies used are listed in chapter 3.4.

4.10 Luciferase assay

H1299 cells were trypsinized and seeded in a 12-well plate with 3×10^4 cells/well and transfected with 100 ng of pGL3-*Wasf1* plasmid, 20 ng of

Renilla reporter plasmid for normalization, and 25 nM *miR-34a* or *miR-34c* pre-miRNAs or a negative control oligonucleotide (Ambion) by using HiPerFect Transfection Reagent (Qiagen). 48 hours later luciferase assays were performed with the Dual-Luciferase Reporter 1000 Assay System (Promega). Fluorescence intensities were measured with an Orion II Microplate Luminometer (Titertek-Berthold).

4.11   FFPE sample preparation

18 weeks old mice were sacrificed and intestine was collected and flushed with cold PBS. The intestine was then opened longitudinally, photographed and rolled up as a "Swiss roll" and placed into at least 10 volumes of 4% buffered formaldehyde. Then the sample cassettes were incubated at 4°C overnight. Dehydration, clearing, and wax infiltration were done by an automated tissue processor. Finally, the tissues were embedded in paraffin.

4.12   Histologic analysis

For each FFPE sample, 3 μm paraffin sections were cut for subsequent immunohistochemistry analysis. H&E staining and periodic acid–Schiff (PAS) staining were performed by an automated slide staining system according to standard protocols. Tumors from *Apc*$^{Min/+}$ mice were classified as adenomas with either low- or high-grade dysplasia, based on nuclear-cytoplasmic ratio, nucleus location, prominence of nucleoli, gland architecture, amount of interglandular stroma, and the presence of mucus secretion.

4.13 Immunohistochemistry

Paraffin sections were de-paraffinized and rehydrated through xylene and graded alcohol series according to standard protocol. Antigen unmasking was performed by immersing tissue sections into pre-heated Citrate Target Retrieval Solution (Agilent Technologies) and a 30 minutes heat-induced target retrieval procedure was carried out. After the tissue sections cooled down to the room temperature, 3% hydrogen peroxide was applied to the sections for 10 minutes to deactivate endogenous peroxidase activities. Then washed the sections with PBS and incubated for 30 minutes with blocking serum or 3% BSA solution. Blocking solution was removed, 100 µl primary antibody diluted in Antibody Diluent with Background-Reducing Components (Agilent Technologies) was added to each section and incubated at 4°C overnight. After washed with PBS, the sections were then incubated with diluted biotinylated secondary antibody for 1 hour. The signal amplification was performed by using VECTASTAIN Elite ABC HRP Kit (Vector Laboratories) and the signal was detected by using DAB Substrate Kit (Vector Laboratories). All antibodies used are listed in chapter 3.4.

4.14 Scoring of immunohistochemical signals

4.14.1 *H*-score

For quantification of MUC1 expression the *H*-score was applied to ≥ 40 tumors per genotype [64]. Each tumor was given an intensity value (I) from 0 to 3 (0, no staining; 1, weak staining; 2, moderate staining; 3, strong staining) and the percentage (Pi) of the tumor area positive for the respective intensity

was recorded from 0 to 100%. The *H*-score was calculated as: *H*-score = Σ (Pi × I) (final range from 0 to 300).

4.14.2 Computerized scoring

For quantification of Vimentin positive area, Image-Pro Plus 6.0 software was used [65]. Section pictures were converted from the RGB color mode to the HSI (Hue-Saturation-Intensity) color mode. The HSI threshold parameters were set to H: 0 - 30; S: 0 - 255; I: 0 - 230 and the area inside this color ranges was counted as positive area.

4.15 *in situ* hybridization

4.15.1 *in situ* hybridization

For detection of intestinal stem cells an *Olfm4*-specific, DIG-labeled RNA probe was generated using a murine *Olfm4* vector in combination with a DIG Northern Starter Kit (Roche). Paraffin sections were de-paraffinized and rehydrated through xylene, graded ethanol series (100%, 95% and 70%), DEPC-treated dH$_2$O and DEPC-treated PBS. The sections were then post fixed in 4% PFA-PBS for 10 minutes. After post-fixation, sections were incubated in 0.1% active DEPC-PBS for 30 minutes and equilibrated in 5X SSC. Thereafter, the sections were pre-hybridized in hybridization buffer at 65°C for 2 hours. Removed hybridization buffer and replaced with new hybridization buffer containing 500 gm/ml of digoxigenin-labeled *Olfm4* probe. The sections were hybridized at 65°C for 48 hours, and then rinsed in 2X SSC for 30 minutes at room temperature, 2X SSC for 1 hour at 60°C, 0.1X SSC for 1 hour at 60°C and equilibrated in Tris/NaCl buffer for 5 minutes. Blocking

solution were applied to the sections and incubated for 30 minutes. Alkaline phosphatase conjugated anti-digoxigenin antibody (Roche) was diluted in blocking solution (1:1000). Blocking solution was removed, replaced with antibody solution and incubated the sections at 4°C overnight. After incubation, the slides were washed with Tris/NaCl buffer and NTM buffer. Color development was performed with BCIP/NBT Liquid Substrate System (Sigma-Aldrich) at room temperature for 48 – 72 hours.

4.15.2 Fluorescence *in situ* hybridization

Fresh paraffin sections were de-paraffinized and rehydrated to DEPC-treated dH_2O as described above. To visualize intestinal bacteria by FISH, 5'-FITC-labeled universal eubacteria probe (EUB338) and 5'-Cy3-labeled negative control probe (NON338) were employed. The probes were synthesized (Metabion), diluted in per-warmed hybridization buffer to a final concentration of 1 ng/µl and added to the sections. The slides were incubated at 50°C overnight. After incubation, tissue sections were washed in pre-warmed hybridization buffer, rinsed in dH_2O and mounted with ProLong Gold antifade reagent (Thermo Fisher Scientific).

4.16 Confocal laser scanning microscopy (CLSM)

Fluorescence pictures were taken by using a LSM 700 Laser Scanning Confocal Microscope with ZEN 2009 software and Plan-Apochromat 20X/0.8 M27 objective. For detection of DIPA signal, the following parameters were set up: laser 405 nm 2.0%; pinhole 33 µm; master gain 565; digital gain 1.20; digital offset 150; pixel dwell 101 µs. For FITC signal, laser 488 nm 2.0%;

pinhole 33 µm; master gain 1060; digital gain 1.20; digital offset 140; pixel dwell 101 µs. For Cy3 signal, laser 555 nm 2.0%; pinhole 33 µm; master gain 740; digital gain 1.20; digital offset 150; pixel dwell 101 µs.

4.17   Sequencing

4.17.1 Sanger sequencing

To verify the sequence of cloned 3'-UTR of *Wasf1*, Sanger sequencing was performed by Applied Biosystems 3130 Genetic Analyzer. BigDye Terminator v1.1 Cycle Sequencing Kit (Thermo Fisher Scientific) was used to perform fluorescence-based cycle sequencing reactions. The components and cycling conditions were as followed:

Reaction mixtures (µl)		Thermocycling conditions		
Component	Vol.	Step	Temp	Time
Ready Reaction Premix 2.5X	4.0	Initial	96°C	1 min
BigDye Sequencing Buffer 5X	2.0	15	96°C	10 sec
Primer 3.2 pmol	1.0	Cycles	60°C	90 sec
Plasmid 1µg	1.0	Hold	4°C	
dH$_2$O	2.0			
Total	10.0			

DyeEx 2.0 Spin Kit (Qiagen) was used to purify the extension products according to the instruction of the manufacturer. Purified products were diluted in Hi-Di Formamide (Thermo Fisher Scientific) and loaded onto Genetic Analyzer for electrophoresis with POP-6 polymer (Thermo Fisher Scientific). Data was collected with Foundation Data Collection Software v3.0 and evaluated with DNAstar v7.1.

4.17.2 Next-Generation Sequencing (NGS)

Total RNA from *Apc*[Min/+] mice and *miR-34a/b/c*[-/-]; *Apc*[Min/+] mice adenomas were isolated. 3 RNA samples per genotype were used for Next-Generation Sequencing and each tumor RNA sample represented a pool of 3 tumors isolated from the same mouse. Random primed cDNA libraries were constructed and sequenced using the HiSeq2500 (Illumina) platform by GATC (Konstanz, Germany). Each sample was covered by at least 35 million single reads of 50 bp length. Data were normalized in R with the RUVSeq [66] module, differential expression analysis was performed using Chipster software 3.7 (http://chipster.csc.fi/) [67]. The overlap of DEseq2 and edgeR results were considered to represent the most differentially expression genes. Gene Ontology (GO) and KEGG pathway analysis was performed with DAVID Bioinformatics Resources (https://david-d.ncifcrf.gov/) [68]. Gene Set Enrichment Analysis (GSEA) was performed using the GSEA software v2.2.2 (http://software.broadinstitute.org/gsea/) [69]. miR-34a/b/c targets were predicted with TargetScan 6.2 (http://www.targetscan.org/) [70]. Expression data was deposited in the Gene Expression Omnibus website (Accession No. GSE84138).

4.18   TCGA-COAD database analysis

The Cancer Genome Atlas (TCGA) [71] gene expression data and follow-up information of colon adenocarcinomas (COAD) were downloaded from NCI's Genomic Data Commons website (GDC; https://gdc.cancer.gov/) [72]. Log_2(Normalized RSEM count + 1) was used to determine the expression of relevant mRNAs. The "normalized RSEM" was already normalized to the

library size and was a more accurate representation of the transcript abundances when compared to the "raw count" [73]. Clinical outcome data were divided into high, intermediate, and low expression groups according to the expression value of individual genes.

4.19   Statistical analysis

A two-tailed Student t test was used to compare continuous variables. Categorical variables were compared using the χ^2 test or Fisher's exact test. Kaplan-Meier calculations were used to display the overall survival time and the results were compared with a log-rank test. The Sidak method was used to adjusted P values when multiple comparisons were performed. P values less than 0.05 were considered significant and indicated by asterisks (*$P <$ 0.05, **$P <$ 0.01, or ***$P <$ 0.0001). Univariate, age/gender/tumor grade-adjusted hazard ratios and 95% confidence intervals (CIs) were estimated with a Cox's proportional hazard model. Prism 6 (GraphPad software) or SPSS (IBM) programs were used for calculations.

5. Results

5.1 *miR-34a/b/c* deletion modulates the architecture of the small intestine in mice

Mice carrying deletions of the *miR-34a* or *miR-34b/c* loci and combinations of these were generated. Genotypes were identified by using PCR and agarose gel electrophoresis. The resulting genotypes were obtained in the expected Mendelian ratios. Deletion of *miR-34a, miR-34b/c* or *miR-34a/b/c* in the germ-line did not significantly influence the lifespan of mice (Figure 7).
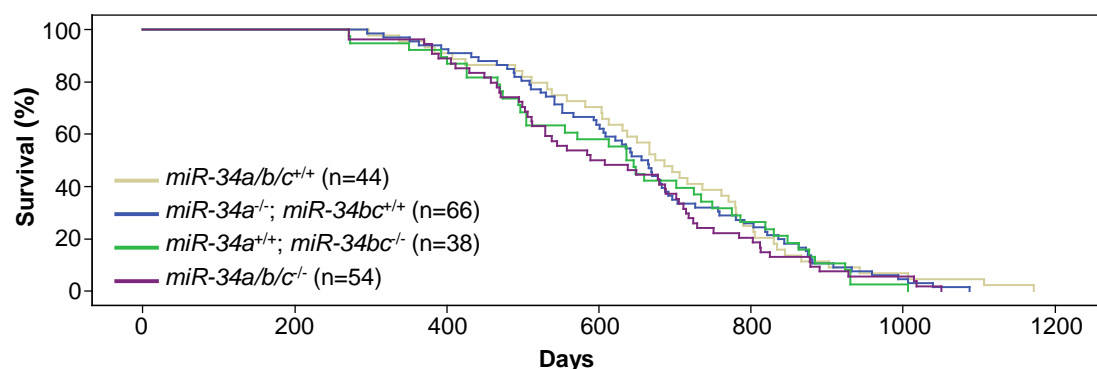
Figure 7.

Kaplan-Meier survival analysis of mice with the indicated genotypes. Results were compared with a log-rank test. *** *P* < 0.001.

However, we observed a gender-independent increase in the width and depth of crypts of the small intestine in *miR-34a/b/c*-deficient mice which presumably caused the minor increase in the total length of the small intestine (Figure 8).
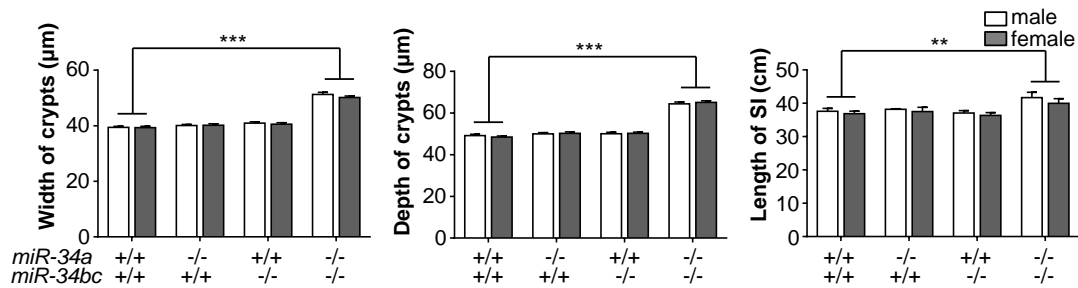
Figure 8.

Determination of the width (left graph) and depth (middle graph) of small intestinal crypts. At least 200 crypts in the jejunum from 18 weeks old mice were analyzed. The length (right graph) of the small intestine was determined in mice with the indicated genotypes (n ≥ 3 mice per gender). ** P < 0.01, *** P < 0.001 (Student's t-test).

Notably, the numbers of Paneth cells per crypt and Goblet cells per villus were significantly increased in female and male *miR-34a/b/c*-deficient mice (Figure 9). In addition, the frequency of stem cells at the crypt base was significantly increased in *miR-34a/b/c*-deficient mice as determined by detection of the stem cell marker *Olfm4* using *in situ* hybridization (Figure 10).

A

B
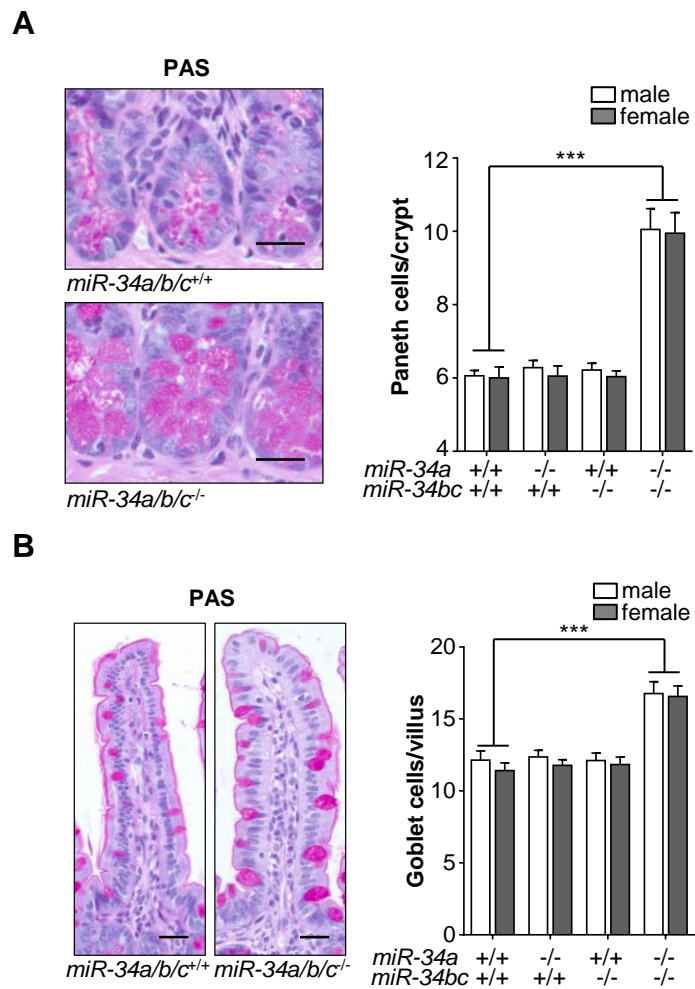
Figure 9.

After PAS staining Paneth cell number per crypt (**A**) and Goblet cell number per villus (**B**) were evaluated in ≥ 50 crypts and ≥ 50 villi per mouse, respectively (n ≥ 3 mice per gender). Scale bar: 25 μm. Results are presented as mean ± SEM. *** $P <$ 0.001 (Student's t-test).
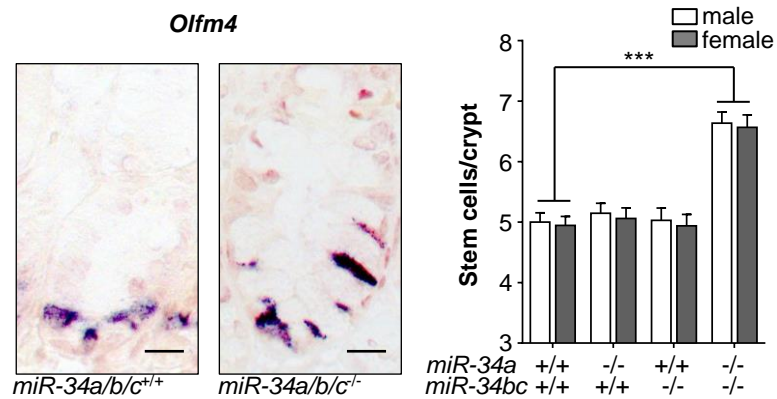
Figure 10.

Representative pictures of in situ hybridization of *Olfm4* positive cells in the crypts from indicated genotypes. At least 50 crypts per mouse were counted (n ≥ 3 mice per gender). Scale bar: 10 μm. Results are presented as mean ± SEM. *** P < 0.001 (Student's t-test).

In order to determine, whether inactivation of *miR-34* genes affects intestinal tumor formation, we generated *Apc*^Min/+ mice with deletions of *miR-34a*, *miR-34b/c* or *miR-34a/b/c*. Genotype was identified by using PCR and agarose gel electrophoresis. In *Apc*^Min/+ mice deficiency for *miR-34a/b/c* also resulted in an increase of the number of Paneth (Figure 11), Goblet and *Olmf4*-positive cells (Figure 12) per crypt in untransformed tissue of the small intestine.

A

PAS

miR-34a/b/c⁺/⁺; Apc^Min/+

miR-34a/b/c⁻/⁻; Apc^Min/+

B

Lysozyme

miR-34a/b/c⁺/⁺; Apc^Min/+   *miR-34a/b/c⁻/⁻; Apc^Min/+*
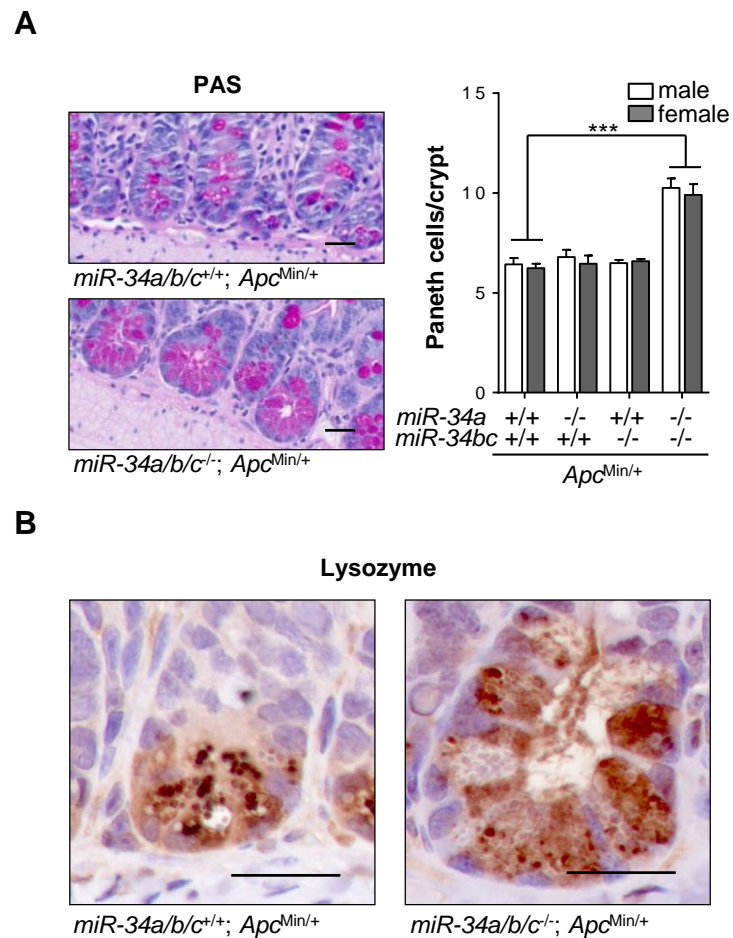
Figure 11.

A. Paneth cell number per crypt after PAS staining was evaluated in ≥ 50 crypts per mouse (n ≥ 5 mice per gender). Scale bar: 25 μm.

B. Detection of Lysozyme expression in Paneth cells. Scale bar: 25 μm.

Results are presented as mean ± SEM. *** $P < 0.001$ (Student's t-test).

A
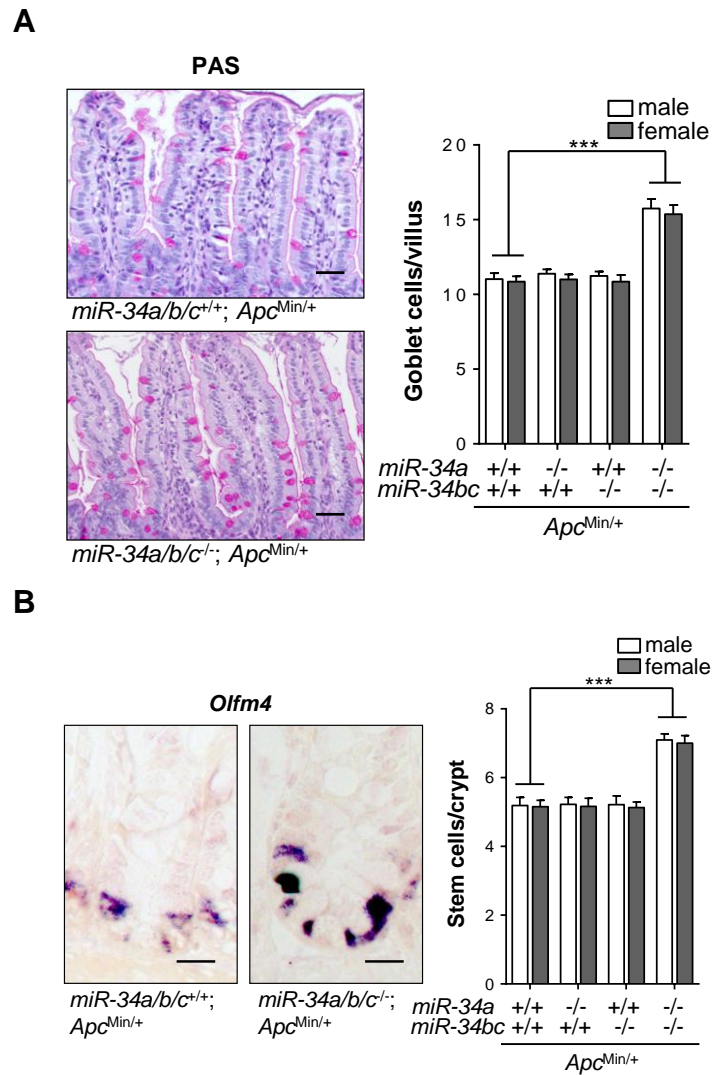
Figure 12.

A. Goblet cell number per villus was evaluated by PAS staining in ≥ 50 villi per mouse (n ≥ 5 mice per gender). Scale bar: 25 µm.

B. Representative examples of *Olfm4* detection by *in situ* hybridization in small intestinal crypts of mice with the indicated genotypes. At least 50 crypts per mouse were counted (n ≥ 5 mice per gender). Scale bar: 10 µm.

Results are presented as mean ± SEM. *** $P < 0.001$ (Student's t-test).

Similarly, the width and depth of the crypts were increased significantly in *miR-34a/b/c*-deficient *Apc*^Min/+ mice, but the minor increased length of the small intestine was not statistically significant (Figure 13). Again, these

architectural changes were observed in both, male and female mice. Therefore, deletion of one *Apc* allele did not influence the morphological changes in the intestine caused by deletion of *miR-34a/b/c*.
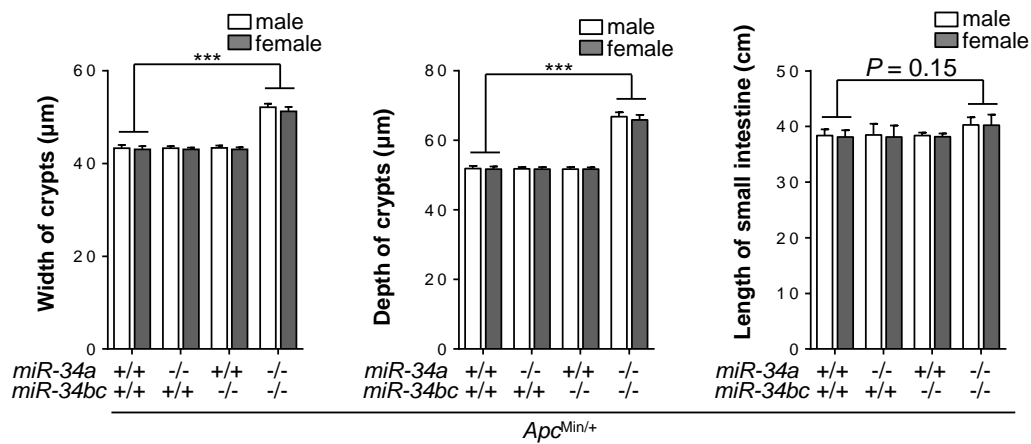
Figure 13.

Determination of the width (left graph) and depth (middle graph) of small intestinal crypts. At least 200 crypts in the jejunum were analyzed. The length of the small intestine was determined in mice with the indicated genotypes (right graph, n ≥ 5 mice per gender). Results are presented as mean ± SEM. *** $P < 0.001$ (Student's t-test).

5.2 *miR-34a/b/c* loss enhances tumorigenesis in *Apc*^Min/+ mice

Notably, *miR-34a/b/c*$^{-/-}$; *Apc*$^{Min/+}$ mice showed signs of morbidity sooner and exhibited a shorter life-span than wild-type *Apc*$^{Min/+}$ mice (Figure 14). In contrast, *Apc*$^{Min/+}$ mice deficient for either the *miR-34a* or the *miR-34b/c* allele did not show a statistically significant change in life-span (Figure 14).
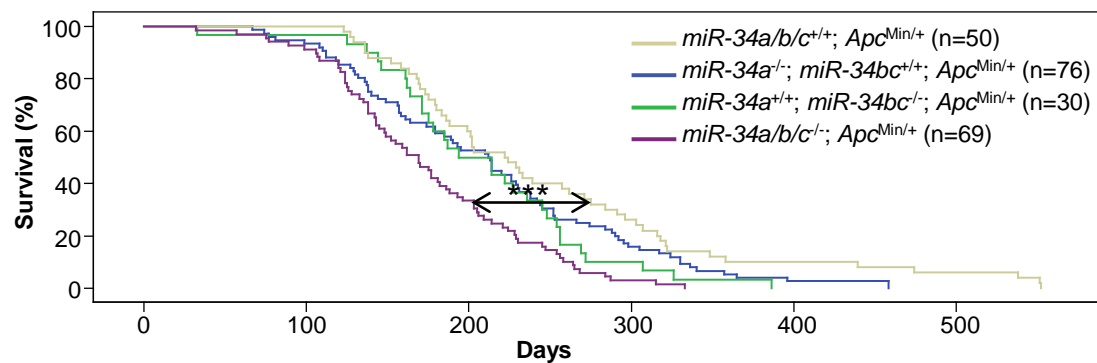
Figure 14.

Kaplan-Meier survival analysis of the indicated genotypes. Results were compared with a log-rank test. *** $P < 0.001$.

When mice were sacrificed at the age of 18 weeks and the entire small intestinal tract was examined (Figure 15), *miR-34a/b/c*$^{-/-}$; *Apc*$^{Min/+}$ and, to a lesser extent, *miR-34a*$^{-/-}$; *Apc*$^{Min/+}$ knockout mice showed a significantly increased number of tumors when compared to *Apc*$^{Min/+}$ mice (Figure 16A). Furthermore, the total tumor area in *miR-34a/b/c*$^{-/-}$; *Apc*$^{Min/+}$ mice was ~4 times larger than in wild-type *Apc*$^{Min/+}$ mice (Figure 16B).
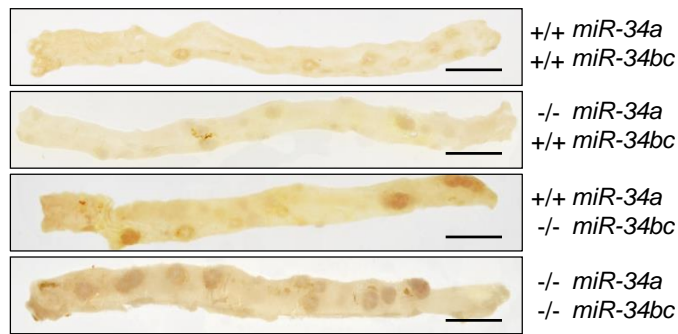
Figure 15.

Representative images of resected small intestines. Scale bar: 1 cm.
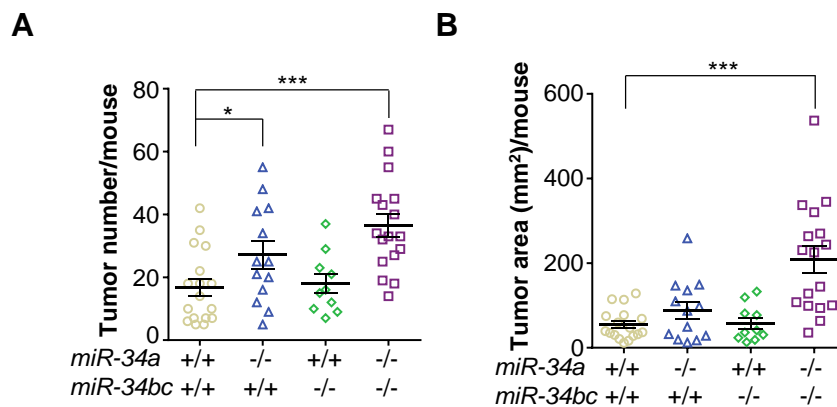
Figure 16.

Quantification of intestinal tumor number (**A**) and tumor area per mouse (**B**) (n ≥ 10 mice per genotype). Results are presented as mean ± SEM. *** $P < 0.001$ (Student's t-test).

The frequency of large tumors (>6 mm^2) was significantly higher when *miR-34a/b/c*, but not when only *miR-34a* or *miR-34b/c* genes had been deleted in *Apc*$^{Min/+}$ mice (Figure 17).
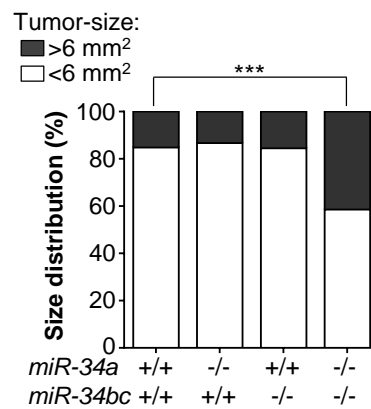
Figure 17.

Graph showing the percentage of tumor size (surface area) distribution in ≥ 100 tumors (n ≥ 10 mice per genotype). *** $P < 0.001$ (Chi-squared test).

We also noted a significantly increased number of adenomas with high-grade dysplasia in *miR-34a/b/c*-deficient *Apc*^Min/+^ mice, whereas the inactivation of either *miR-34a* or *miR-34b/c* alone did not have this effect (Figure 18).

A

B
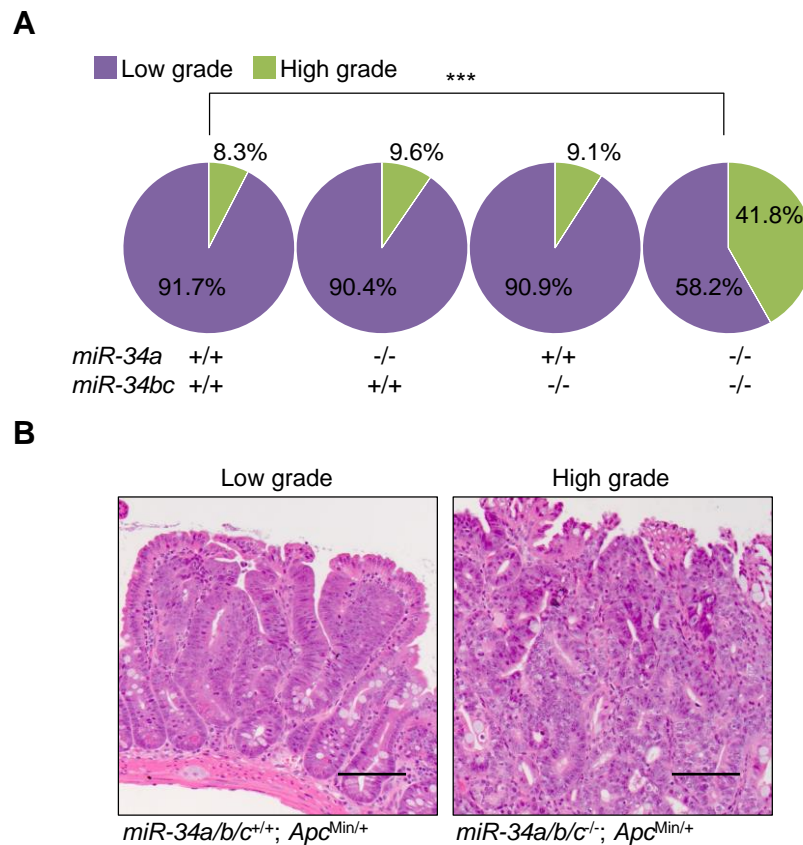
Figure 18.

A. Tumor stage (low grade adenoma, high grade adenoma) of ≥ 66 intestinal tumors (n ≥ 10 mice per genotype). *** $P < 0.001$ (Chi-squared test).

B. Representative images of low and high grade adenomas. Scale bar: 100 µm.

Taken together, our findings show that the inactivation of *miR-34a/b/c* promotes intestinal tumor formation by increasing tumor initiation and enhancing the growth of tumors in *Apc*Min/+ mice. As the combined inactivation of *miR-34a* and *miR-34b/c* genes was necessary for these effects, these miRNAs may have overlapping functions and compensate each other. In addition, these results are in accordance with the combined epigenetic inactivation of *miR-34a* and *miR-34b/c* by DNA methylation, which has been detected in more than 75% of analyzed CRC samples [38]. In the subsequent

analyses, we therefore focused on studying mice with simultaneous deletion of *miR-34a* and *miR-34b/c*.

5.3 *miR-34a/b/c* loss affects proliferation, apoptosis and infiltration by bacteria and immune cells of adenomas

Notably, tumors in *miR-34a/b/c* knockout *Apc*$^{Min/+}$ mice showed a significant increase in proliferation and a significantly reduced rate of apoptosis (Figure 19). The frequency of stromal cells within the tumors was not affected by *miR-34a/b/c* deletion as determined by detection of Vimentin (Figure 20).
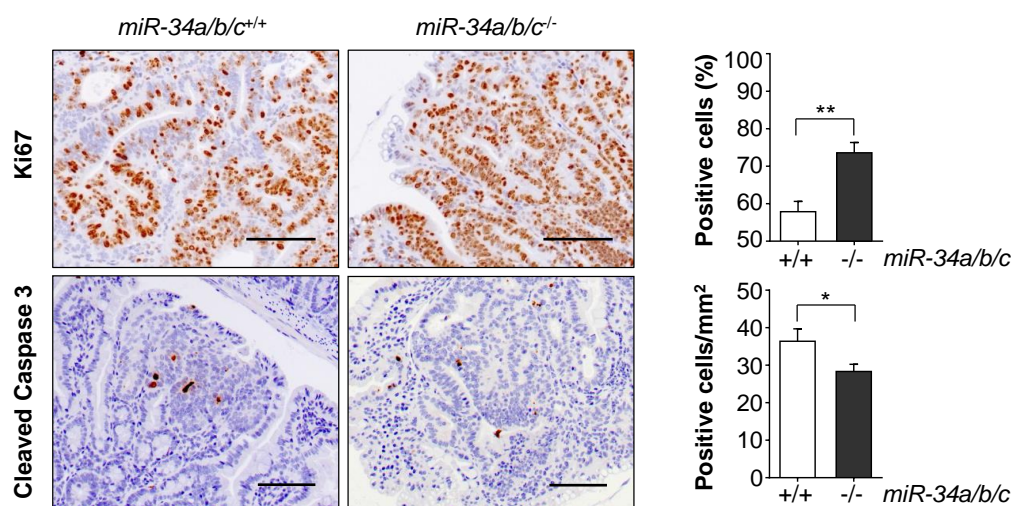
Figure 19.

IHC detection of Ki67 and cleaved-caspased-3 in adenomas from 18 weeks old *Apc*$^{Min/+}$ mice with the indicated genotypes. (n = 7 mice per genotype). Results are presented as mean ± SEM. * *P* < 0.05, ** *P* < 0.01 (Student's t-test). Scale bar: 100 µm.
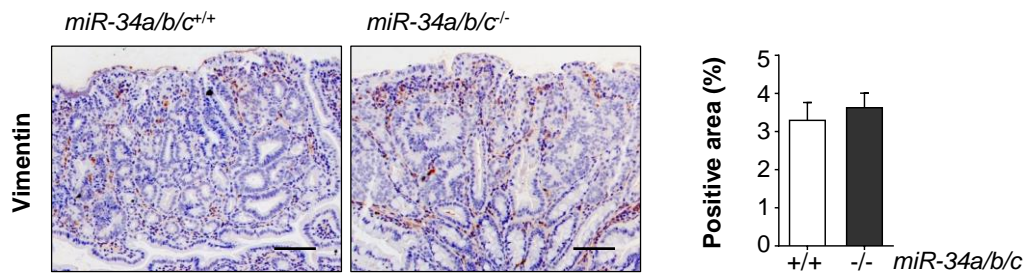
Figure 20.

Detection of Vimentin expression by immunohistochemistry in adenomas with the indicated genotypes. (n = 7 mice per genotype). Scale bar: 100 µm.

Because it was recently shown that bacterial infiltration promotes tumorigenesis in *Apc*[Min/+] mice [74], we asked whether *miR-34a/b/c* deletion affects the presence of bacteria in intestinal tumors. By detection of bacterial 16S rRNA, we found that adenomas from *miR-34a/b/c*[-/-]; *Apc*[Min/+] mice display extensive bacterial infiltration regardless of tumor size or tumor grade (Figure 21). However, the adjacent normal intestinal epithelium of all mice analyzed here was devoid of bacteria. Therefore, *miR-34a/b/c*-deficient mice do not display a general intestinal barrier defect.

A

B
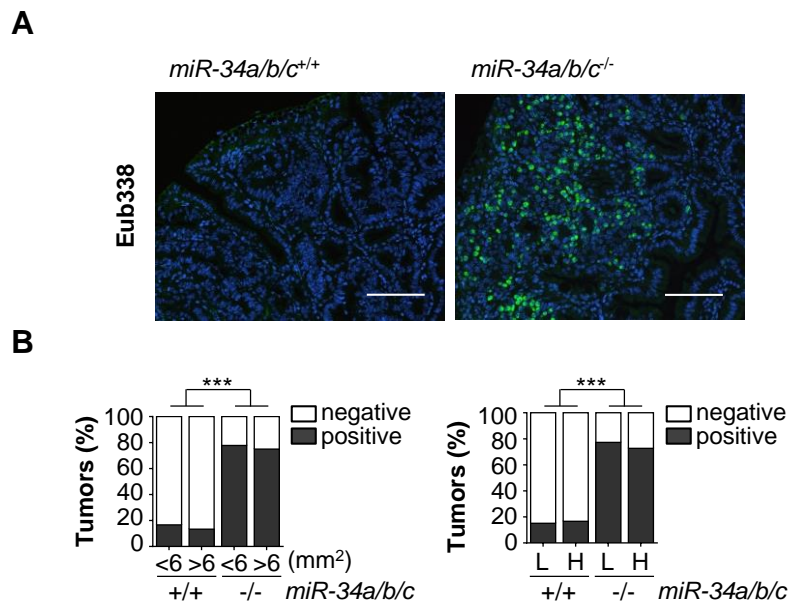
Figure 21.

A. Fluorescence *in situ* hybridization (FISH) with a universal eubacterial probe (EUB338) in adenomas from 18 weeks old *Apc*^Min/+ mice with the indicated genotypes. (n = 7 mice per genotype). Scale bar: 100 μm.

B. Evaluation of EUB338 probe positive rate in different sizes (left panel) and different grades (right panel) adenomas. (n = 7 mice per genotype). *** $P < 0.001$ (Fisher's exact test).

Unexpectedly, the frequency of immune cells, such as macrophages, T- and B-cell, was decreased in *miR-34a/b/c*-deficient adenomas (Figure 22). Therefore, the increased bacterial infiltration of adenomas may be due to a defect in the tumor-associated immune defense in *miR-34a/b/c*-deficient mice.
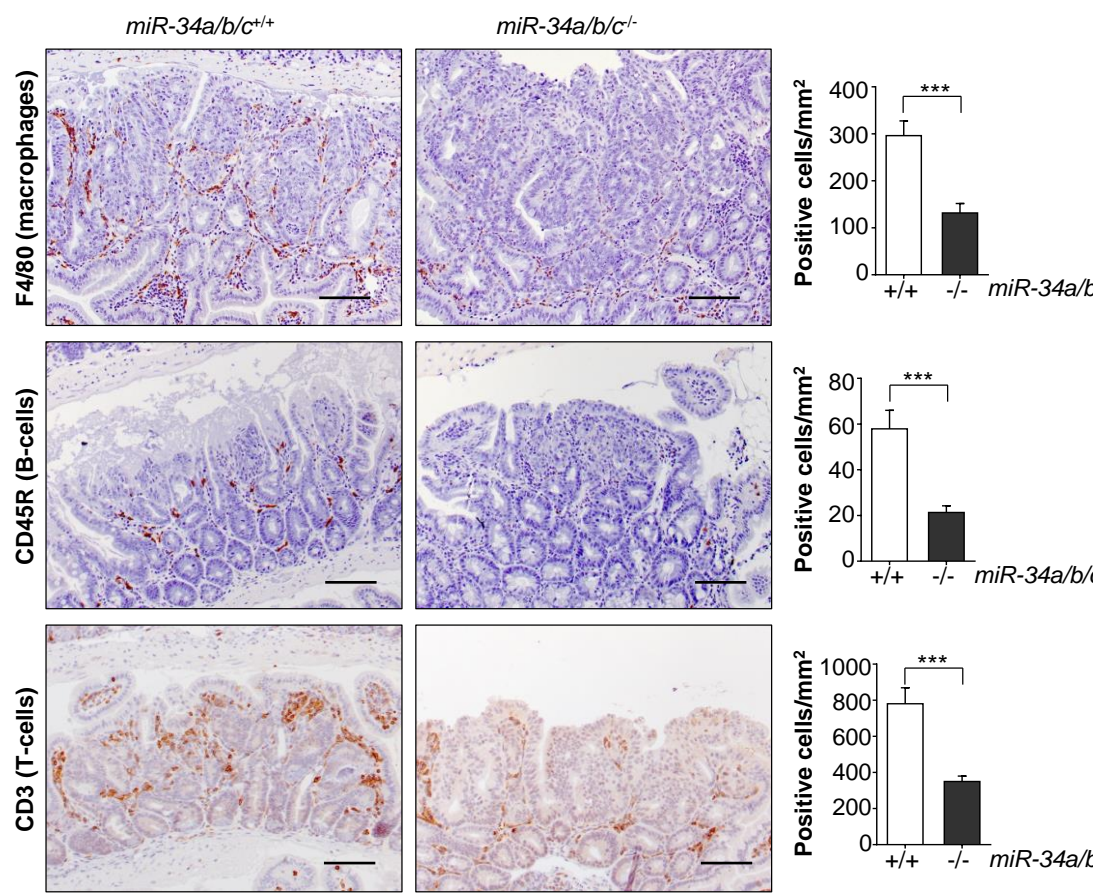
Figure 22.

Quantification of infiltrated macrophages, B and T cells by F4/80, CD45R and CD3 immuno-detection respectively in adenomas. (n ≥ 10 mice per genotype). Results are presented as mean ± SEM. *** $P < 0.001$ (Student's t-test). Scale bar: 100 μm.

5.4 Expression profiling of *miR-34a/b/c*-deficient adenomas

To further illuminate the mechanisms by which *miR-34a/b/c* loss promotes intestinal tumorigenesis in *Apc*[Min/+] mice we obtained mRNA expression profiles of adenomas from 18-weeks old *miR-34a/b/c*-deficient *Apc*[Min/+] mice and wild-type *Apc*[Min/+] mice. For each mouse (n=3 per genotype) RNAs derived from 3 different tumors were pooled, libraries were generated and subjected to RNA-Seq to obtain more than 35 million reads per library. Thereby we detected the up-regulation of 1773 mRNAs, when mRNAs with a $|\log_2(\text{fold change})| \geq 0.6$ and RPKM ≥ 0.25 in *miR-34*a/b/c[-/-]; *Apc*[Min/+] mice versus wild-type *Apc*[Min/+] mice were included (Figure 23). As expected, the percentage of mRNAs up-regulated in the *miR-34a/b/c*-deficient tumors was higher for mRNAs harboring miR-34a/b/c seed-matching sequences than for mRNAs lacking these (Figure 24).
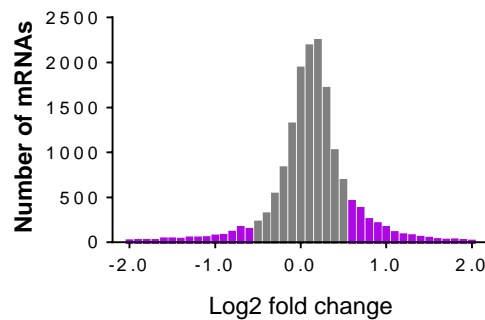
Figure 23.

Results of NGS analysis represented as histogram showing changes in mRNA levels after *miR-34a/b/c* deletion. Transcriptionally regulated genes with a $|\log_2(\text{fold change})| \geq 0.6$ and RPKM ≥ 0.25 are highlighted as purple bars. Fold change denotes the ratio of mRNA expression values in tumors of *miR-34a/b/c*[-/-]; *Apc*[Min/+] mice vs. *miR-34a/b/c*[+/+]; *Apc*[Min/+] mice (n = 3 mice per genotype).
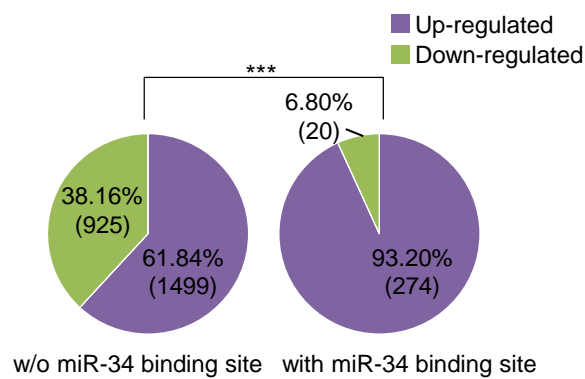
Figure 24.

Calculation of the percentage of mRNAs differentially regulated in *miR-34a/b/c*-deficient vs. wild-type tumors in *Apc*^{Min/+} mice without (left graph) and with (right graph) miR-34a/b/c seed-matching sequences. *** $P < 0.001$.

324 mRNAs were identified as differentially regulated due to *miR-34a/b/c* loss when the raw-count methods DESeq2 [75] and edgeR [76] were applied (Figure 25). After unsupervised clustering of these differentially expressed genes one of the *miR-34a/b/c*-deficient tumor samples showed a divergent expression profile, which was presumably due to biological variation (Figure 26).
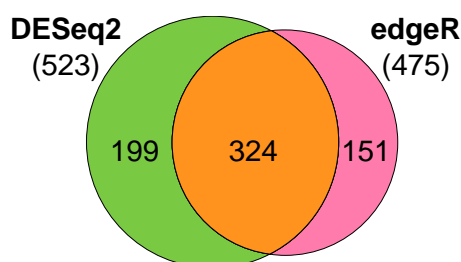
Figure 25.

Results of DESeq2 and edgeR analyses of the NGS results.
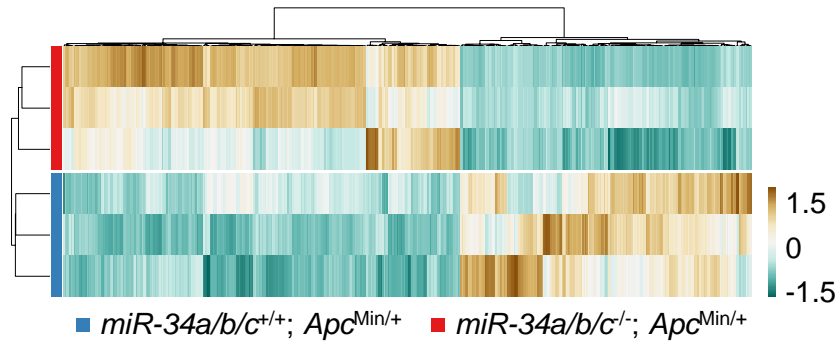
Figure 26.

Heatmap of genes with significantly differential expression in tumors from mice with the indicated genotypes. Differential gene expression is shown according to the pseudocolor scale indicated on the right side.

Next, we used Gene Ontology (GO) and KEGG pathway analyses to group the differentially expressed transcripts into functional classes. The GO analysis indicated that the up-regulated mRNAs are involved in cell adhesion, extracellular matrix and growth factor binding functions (Figure 27). The KEGG analysis showed that several pathways were significantly enriched, such as focal adhesion, ECM-receptor interaction, and pathways related to cancer (Figure 28).
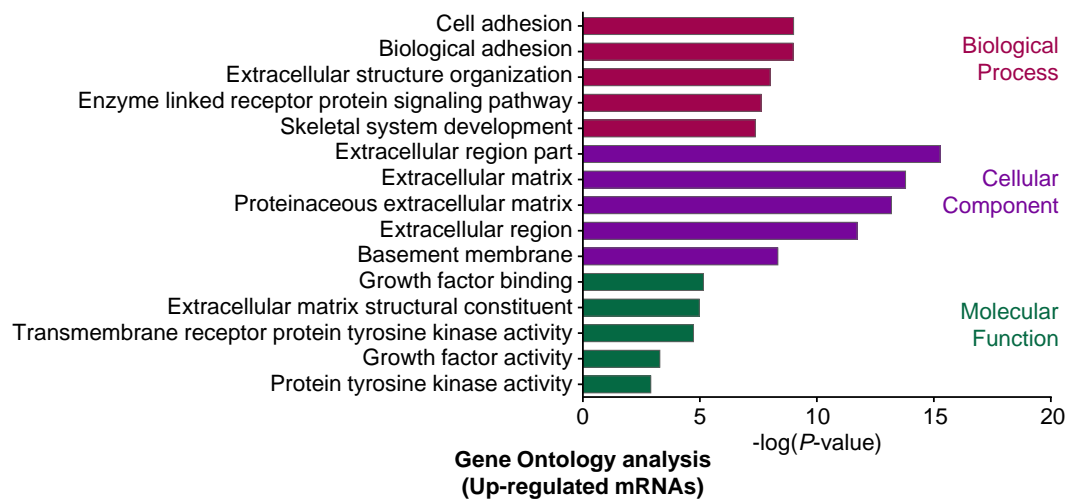
Figure 27.

Top 5 Gene Ontology terms that were most significantly enriched among up-regulated mRNAs of tumors from *miR-34a/b/c*[-/-]; *Apc*[Min/+] mice.
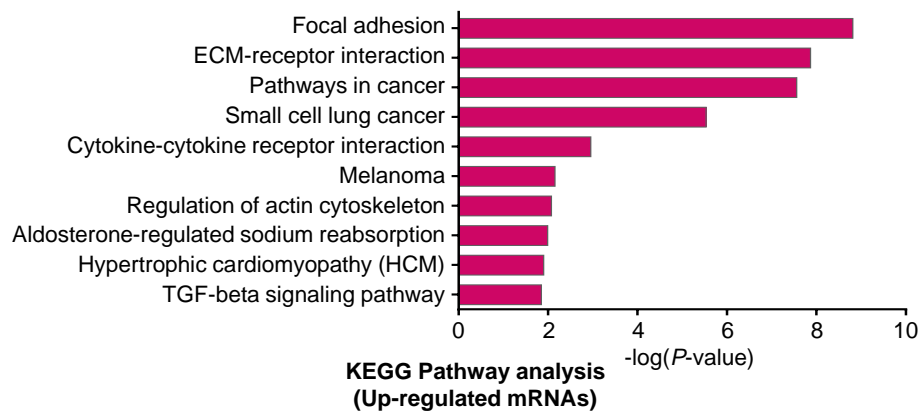
Figure 28.

Top 10 KEGG pathways that were most significantly enriched among up-regulated mRNAs of tumors from *miR-34a/b/c*[-/-]; *Apc*[Min/+] mice.

On the contrary, both GO and KEGG analyses indicated that the down-regulated genes are mainly involved in immune response functions (Figure 29 and Figure 30).
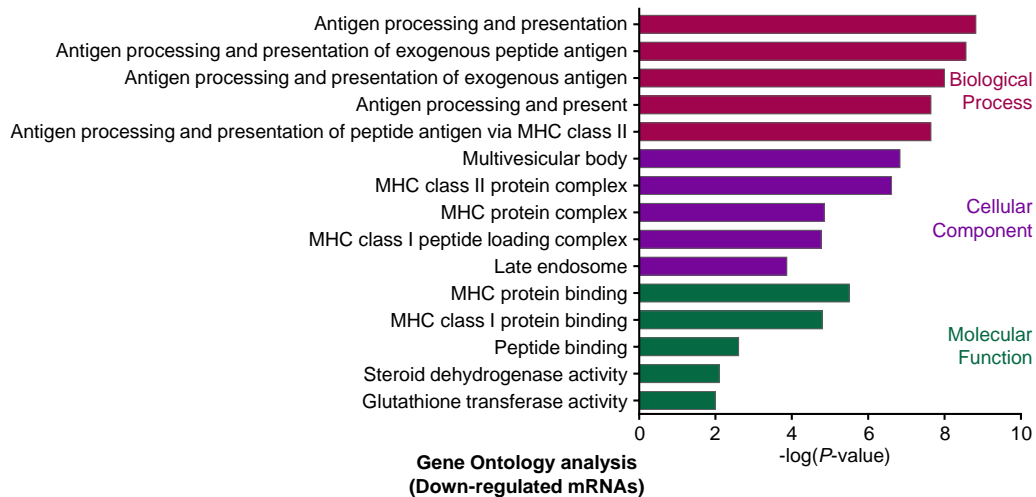
Figure 29.

Top 5 Gene Ontology terms that were most significantly enriched among down-regulated mRNAs of tumors from *miR-34a/b/c⁻/⁻*; *Apc*^Min/+ mice.
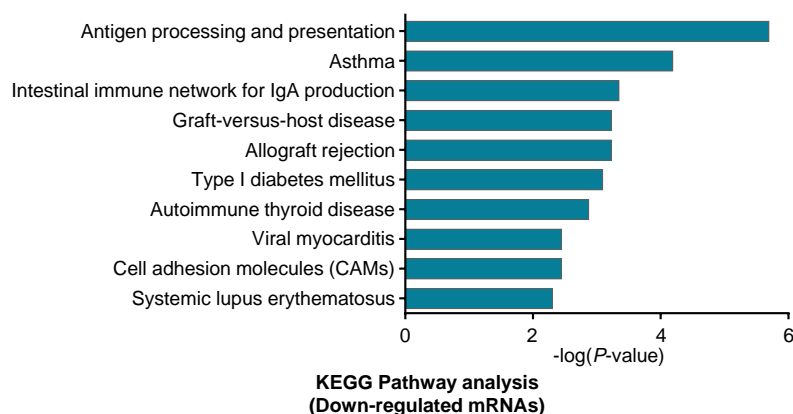
Figure 30.

Top 10 KEGG pathways that were most significantly enriched among down-regulated mRNAs of tumors from *miR-34a/b/c⁻/⁻*; *Apc*^Min/+ mice.

A subsequent Gene Set Enrichment Analysis (GSEA) revealed that *miR-34a/b/c* deletion results in gene expression signatures related to epithelial-mesenchymal-transition (EMT), hypoxia, angiogenesis, inflammatory response, Kras signaling, and apical junction processes (Figure 31).

Interestingly, the expression signatures of *miR-34a/b/c*-deficient adenomas also showed a significant overlap with signatures of intestinal stem cells (ISC) [77], Lgr5^{+} positive cells [78] and the GO Wnt signaling signature.
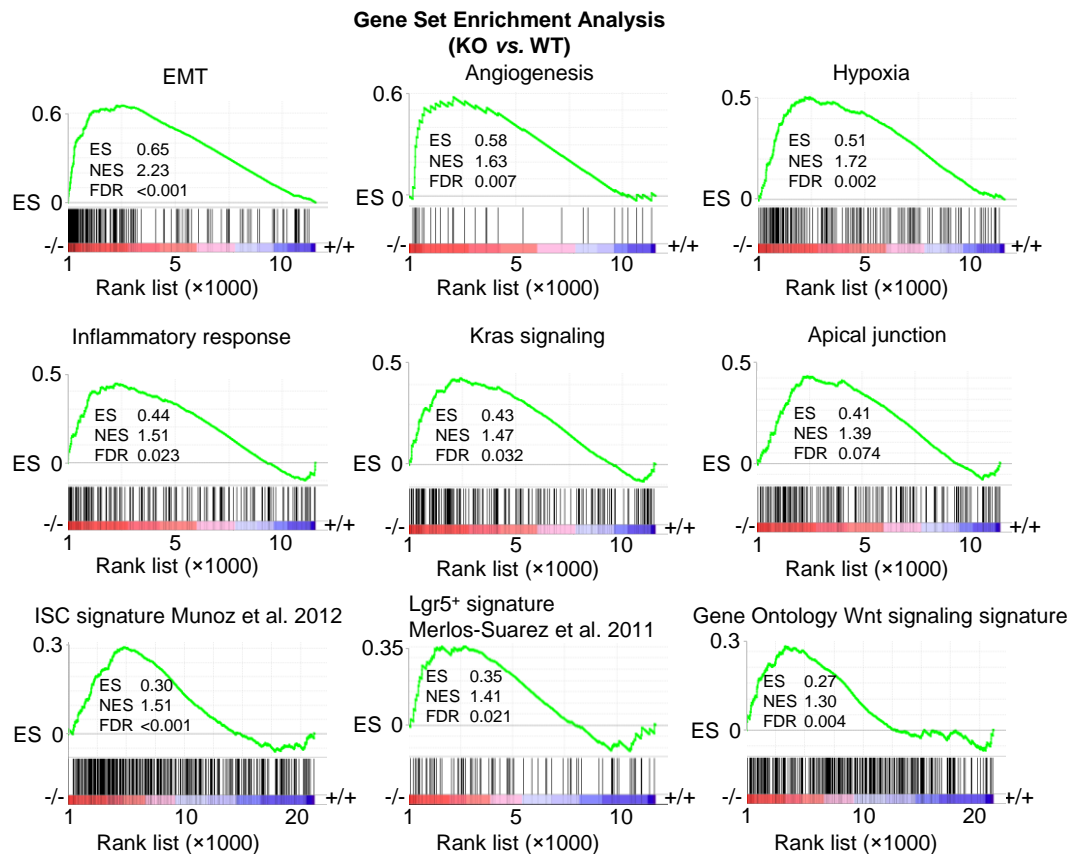
Figure 31.

GSEA analysis of mRNA profiles from tumors of *miR-34a/b/c*[-/-]; *Apc*[Min/+] mice vs. *miR-34a/b/c*[+/+]; *Apc*[Min/+] mice.

In addition, several regulators of barrier function in IEC were also detected as down-regulated by NGS analysis in *miR-34a/b/c*-deficient adenomas (e.g. *Muc1*, *Tff3* and *Retnlb*; fold change: -4.74, -1.44 and -3.34, respectively). The down-regulated mRNA expression of these barrier components was validated by qPCR (Figure 32A). Furthermore, we confirmed the decreased protein expression of MUC1 in *miR-34a/b/c*-deficient

adenomas by immunohistochemistry (Figure 32B). The repression of these barrier components may also contribute to the observed infiltration of bacteria into *miR-34a/b/c*-deficient adenomas.
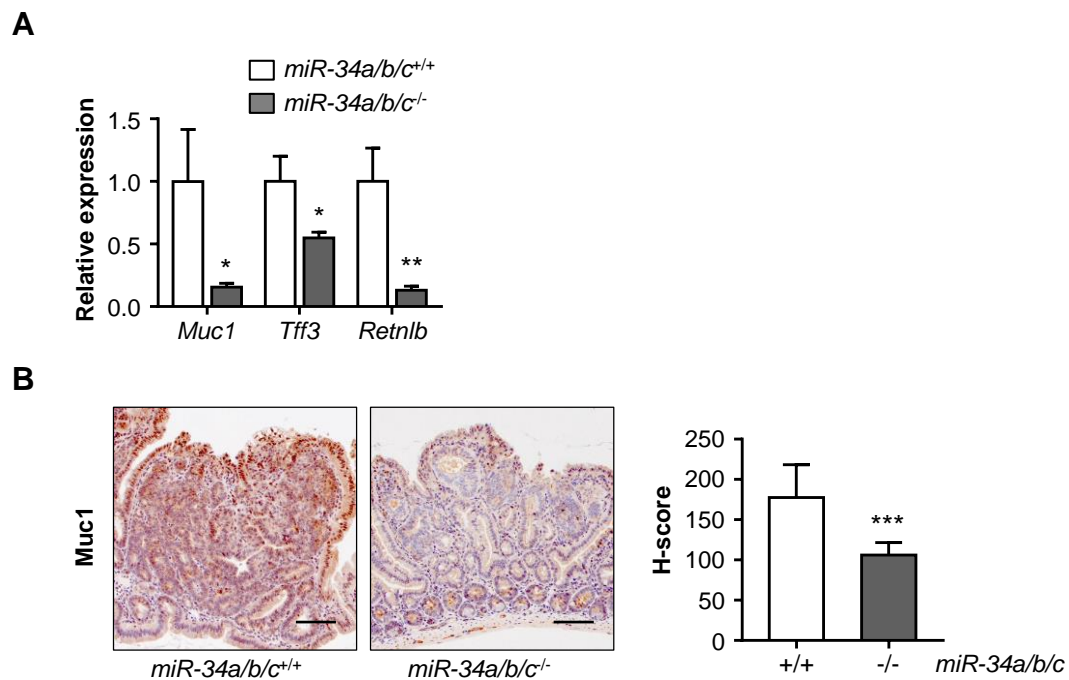
Figure 32.

A. mRNA expression of barrier protein in adenomas from mice with the indicated genotypes (3 tumors per mouse) were determined by qPCR (n = 3 mice per genotype).

B. Detection of MUC1 expression by immunohistochemistry (n ≥ 10 mice per genotype). Left panels: Representative examples of MUC1 detection in adenomas from mice with the indicated genotypes. Scale bar: 100 µm. Right panel: Evaluation of MUC1 expression using the *H*-score.

Results in A and B are presented as mean ± SD. * $P < 0.05$, ** $P < 0.01$, *** $P < 0.001$ (Student's t-test).

5.5 *miR-34a/b/c* loss enhances the formation of intestinal tumor organoids

To obtain functional evidence for an enhanced stemness of adenoma cells with deletion of *miR-34a/b/c* we performed a tumor organoid formation assay. Indeed, an increased tumor organoid formation rate was observed for *miR-34a/b/c*-deficient adenoma derived cells when compared to those derived from *miR-34a/b/c*-proficient adenomas (Figure 33).

*miR-34a/b/c+/+; Apc*Min/+   *miR-34a/b/c-/-; Apc*Min/+
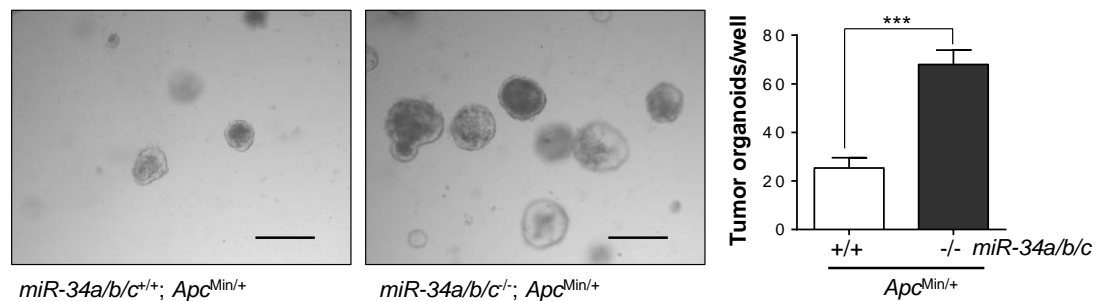
Figure 33.

Tumor organoid formation assay of adenomas (3 tumors per mice) from mice with the indicated genotypes (n = 2 mice per genotype). Scale bar: 200 µm. Results are presented as mean ± SEM. *** *P* < 0.001 (Student's t-test).

5.6 *miR-34a/b/c* deletion enhances intestinal Wnt signaling in *Apc*Min/+ mice

Wnt/β-catenin signaling is critically involved in regulating the homeostasis and neoplastic transformation of the intestine. Since *miR-34a/b/c*-deficient adenomas showed a Wnt signaling signature (Figure 31) and the Wnt/β-catenin pathway is directly regulated by miR-34a/b/c [54] and by APC, we determined whether the expression of β-catenin is also affected in the intestinal epithelial cells of *miR-34a/b/c* knockout mice. Interestingly, we detected an increased nuclear accumulation of β-catenin/CTNNB1 protein in normal crypts after *miR-34a/b/c* deletion in *Apc*Min/+ mice, but not in *miR-34a/b/c*-deficient wild-type mice (Figure 34), indicating that *miR-34a/b/c* deficiency in the presence of hemizygous *Apc* allows the nuclear accumulation of β-catenin in untransformed cells including the stem cells located at the crypt base which represent the preferred cells of origin for intestinal adenomas [79]. Therefore, this effect of *miR-34a/b/c* loss may explain or at least contribute to the increased rate of tumor initiation in *miR-34a/b/c*-deficient *Apc*Min/+ mice.
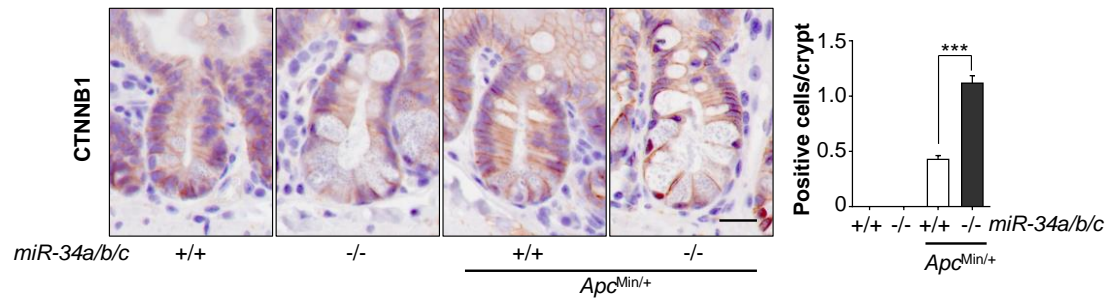
Figure 34.

Detection of β-catenin localization. The number of nuclear β-catenin-positive cells was counted in ≥ 200 crypts (n = 5 mice per genotype). Scale bar: 20 µm. Results are presented as mean ± SEM. *** $P < 0.001$ (Student's t-test).

5.7 Validation of miR-34a/b/c target expression

By bioinformatics analyses of the mRNA profiles obtained here we identified a set of 11 up-regulated mRNAs with miR-34 seed-matching sites in their 3'-UTR which may, at least in part, mediate the tumor suppressive function of miR-34a/b/c (Table 1 and Figure 35).

Table 1. Subset of selected, up-regulated mRNAs with miR-34 seed-matching sequences

Symbol	Full Name	Transcript ID
Pdgfra	platelet derived growth factor receptor, alpha polypeptide	ENSMUST00000000476.9
Pdgfrb	platelet derived growth factor receptor, beta polypeptide	ENSMUST00000025522.5
Axl	AXL receptor tyrosine kinase	ENSMUST00000002677.5
Wasf1	WAS protein family, member 1	ENSMUST00000105509.1
Fgfr1	fibroblast growth factor receptor 1	ENSMUST00000179592.2
Igf1	insulin-like growth factor 1	ENSMUST00000105300.3
Stc1	stanniocalcin 1	ENSMUST00000014957.8
Cacna2d2	calcium channel, voltage-dependent, alpha 2/delta subunit 2	ENSMUST00000010210.7
Col6a2	collagen, type VI, alpha 2	ENSMUST00000001181.7
Col4a2	collagen, type IV, alpha 2	ENSMUST00000033899.8
Inhbb	inhibin beta-B	ENSMUST00000038765.5
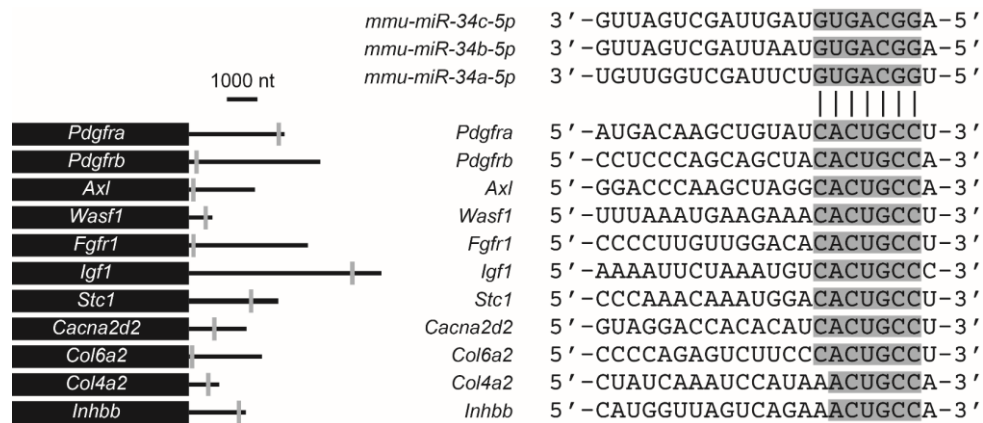
Figure 35.

Positions of miR-34 seed-matching sequences (grey vertical bars) within selected mRNAs (left panel). 3'-UTR sequences of the miR-34 binding site of the selected mRNAs are given in 5'- to 3'- orientation (right panel).

These mRNAs and a selected set of mRNAs with known pro-tumorigenic functions were analyzed by qPCR to exemplarily validate the NGS results (Figure 36). Several of these factors have already been characterized as direct miR-34 targets by others and us (*Pdgfra* [80], *Pdgfrb* [80], and *Axl* [56]). In addition, components of the Wnt pathway and EMT regulators were analyzed. Notably, all of the tested mRNAs were expressed at significantly higher levels in the tumors of *miR-34a/b/c* knockout *Apc*Min/+ mice. Therefore, our screen identified numerous additional miR-34a/b/c targets, which may be up-regulated in CRC and relevant for tumor progression.
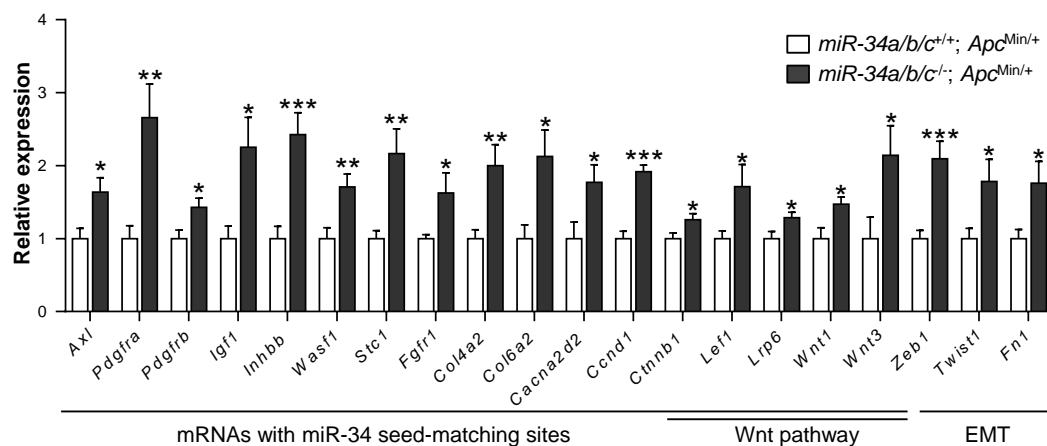
Figure 36.

mRNA expression of selected genes in tumors from mice with the indicated genotypes (3 tumors per mouse) were determined by qPCR (n = 3 mice per genotype). Results are presented as mean ± SD. * $P < 0.05$, ** $P < 0.01$, *** $P < 0.001$ (Student's t-test).

Next, we performed an exemplary characterization of *Wasf1* as a direct miR-34a/b/c target, since *Wasf1* is known to regulate cancer-relevant processes [81]. A luciferase-based reporter containing the full-length 3'-UTR of the murine *Wasf1* mRNA was significantly repressed by co-transfection of *pre-miR-34a* or *pre-miR-34c* (Figure 37). In addition, we detected a significant reduction of *Wasf1* mRNA expression after ectopic expression of *pri-miR-34a* in SW620 CRC cells (Figure 38A). The WASF1 protein showed a delayed repression 72 hours after activation of the *pri-miR-34a* allele which may be due to an unusually stable WASF1 protein (Figure 38B).
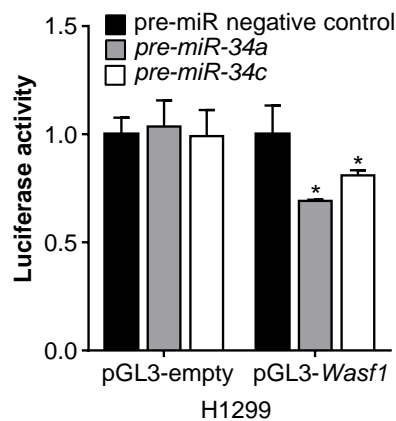
Figure 37.

Dual reporter assay in H1299 cells co-transfected with *pre-miR-34a* mimics, *pre-miR-34c* mimics or control oligonucleotides and *Wasf1* 3'-UTR-reporter constructs (n = 3). Results are presented as mean ± SD. * $P < 0.05$ (Student's t-test).
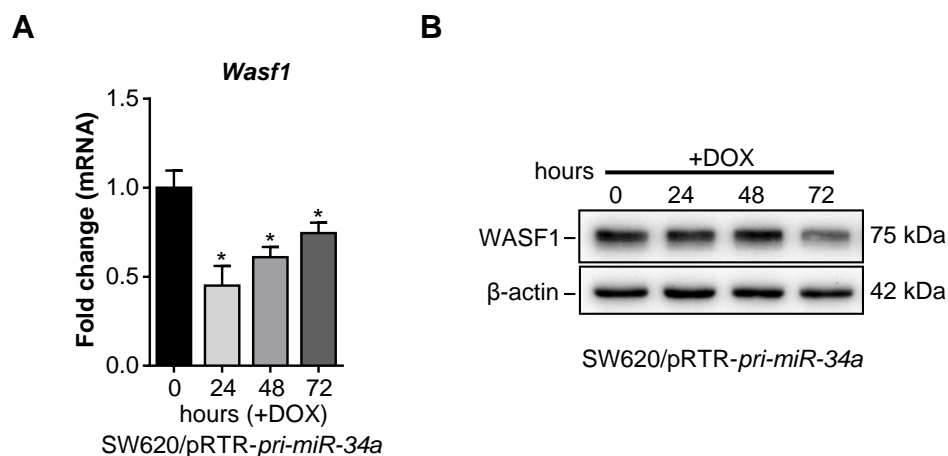
Figure 38.

A. Detection of *Wasf1* mRNA by qPCR after addition of DOX for the indicated periods to SW620/pRTR-*pri-miR-34a* cells (n = 3). Results are presented as mean ± SD. * $P < 0.05$ (Student's t-test).

B. Western blot analysis of WASF1 after activation of ectopic *pri-miR-34a* expression for the indicated periods in SW620/pRTR-*pri-miR-34a* cells (n = 3).

Consistent with being a miR-34a/b/c target, the WASF1 protein showed increased expression in three out of four tumors isolated from *miR-34a/b/c*

knockout $Apc^{Min/+}$ mice, when compared to miR-34a/b/c-proficient tumors (Figure 39). Taken together, these results show that *Wasf1* is a direct target of miR-34a/b/c.
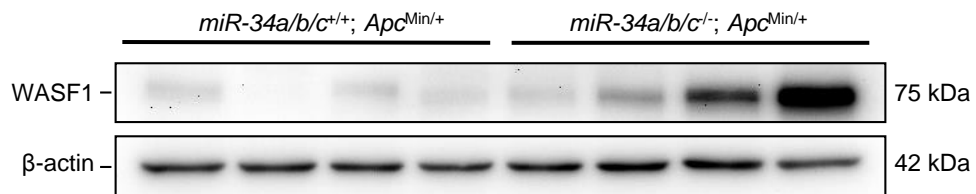
Figure 39.

Western blot analysis of WASF1 expression in tumors from *miR-34a/b/c$^{-/-}$; Apc$^{Min/+}$* mice or *miR-34a/b/c$^{+/+}$; Apc$^{Min/+}$* mice (n = 4 mice per genotype).

5.8 Increased expression of miR-34a/b/c targets in human CRCs is associated with poor survival

In order to determine whether the miR-34 targets described above are also clinically relevant, we analyzed their expression within the expression profiles of 460 human colorectal adenocarcinomas deposited in The Cancer Genome Atlas (TCGA) database [71]. Interestingly, *INHBB, PDGFRB*, *STC1* and *COL4A2* showed a significantly elevated expression in primary CRCs (Figure 40).
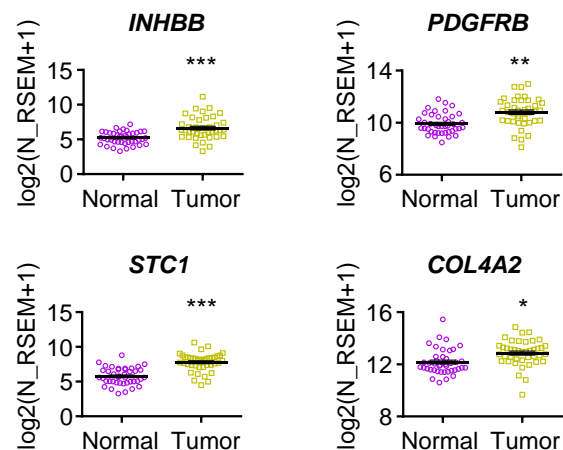
Figure 40.

Expression of selected miR-34 targets in tumor and matched normal tissue in the TCGA collection of COAD (n = 41 patients). Results are presented as mean ± SEM. * $P < 0.05$, ** $P < 0.01$, *** $P < 0.001$ (Paired Student's t-test).

Furthermore, a significantly increased expression of *INHBB, AXL, FGFR1* and *PDGFRB* was detected in primary CRCs from patients with nodal status N2 when compared to samples from patients with lower nodal status (Figure 41). Except for *AXL,* a significantly increased expression of these mRNAs was associated with an increased tumor stage (Figure 42).
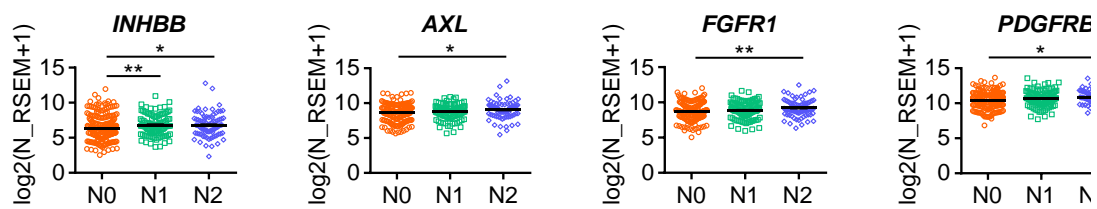
Figure 41.

Correlation of selected mRNA expression in tumor with nodal status (n = 460 patients). Results are presented as mean ± SEM. * $P < 0.05$, ** $P < 0.01$ (Student's t-test).
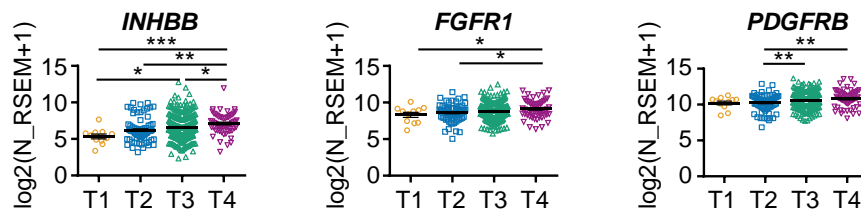
Figure 42.

Correlation of selected mRNA expression with tumor stage (n = 460 patients). Results are presented as mean ± SEM. * $P < 0.05$, ** $P < 0.01$, *** $P < 0.001$ (Student's t-test).

In addition, increased expression of *INHBB* and *AXL* in primary CRCs was significantly associated with decreased patient survival (Table 2 and Figure 43). Elevated expression of *COL4A2, WASF1, STC1* and *PDGFRB* was also associated with poor survival, although not significantly (Figure 43). Since poor survival is mostly due to metastatic spread, these results suggest that the elevated expression of these mRNAs, which may be due to loss of *miR-34a/b/c,* promotes metastasis.

Table 2. Univariate and age/gender/tumor grade-adjusted Cox proportional hazard analysis of selected up-regulated mRNAs with miR-34 seed-matching sequences and overall-survival in the TCGA COAD cohort

mRNA	Univariate			Age/gender/tumor grade-adjusted		
	HR	(95% CI)	*P*	HR	(95% CI)	*P*
Col4a2	1.211	(0.952-1.539)	0.118	1.170	(0.917-1.494)	0.207
Fgfr1	1.101	(0.866-1.399)	0.434	1.048	(0.823-1.334)	0.703
Axl	1.276	(1.014-1.607)	0.038	1.269	(1.007-1.600)	0.044
Stc1	1.199	(0.944-1.523)	0.136	1.133	(0.887-1.447)	0.318
Pdgfrb	1.160	(0.912-1.474)	0.226	1.150	(0.901-1.469)	0.261
Cacna2d2	0.868	(0.680-1.109)	0.258	0.883	(0.689-1.131)	0.324
Igf1	0.990	(0.777-1.261)	0.933	1.040	(0.813-1.331)	0.756
Col6a2	1.077	(0.845-1.373)	0.547	1.079	(0.844-1.378)	0.545
Pdgfra	0.859	(0.679-1.087)	0.206	0.922	(0.724-1.175)	0.512
Inhbb	1.486	(1.152-1.916)	0.002	1.338	(1.028-1.742)	0.030
Wasf1	1.200	(0.945-1.522)	0.134	1.125	(0.884-1.432)	0.338

HR: hazard ratio, CI: confidence interval, COAD: colon adenocarcinoma
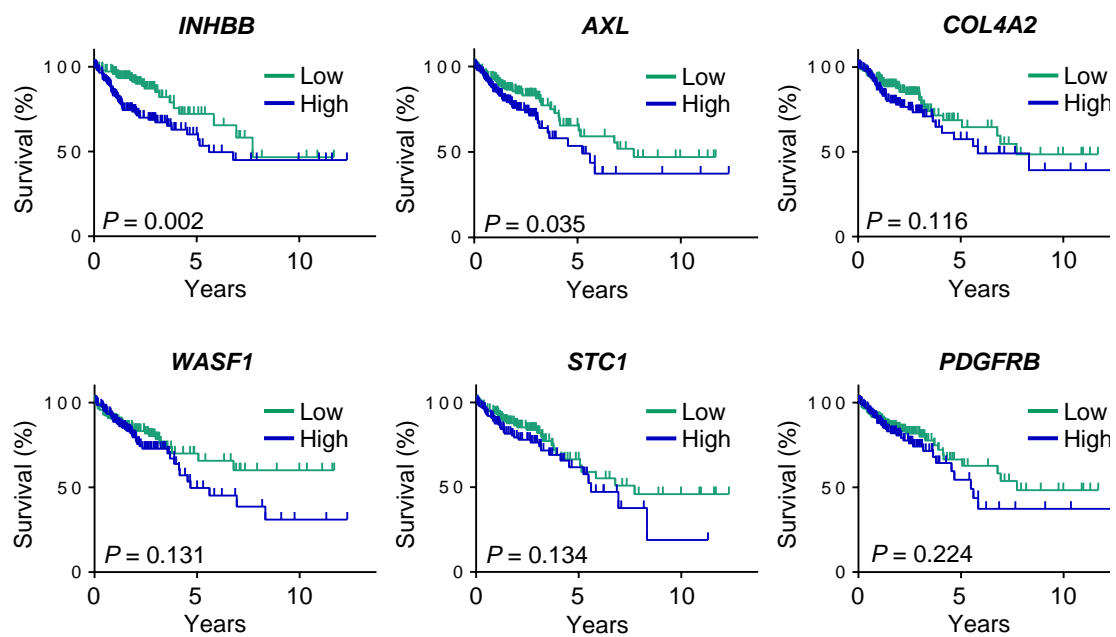
Figure 43.

Kaplan-Meier analysis of overall survival (n = 306 patients). Results were compared with a log-rank test.

Finally, we compiled the regulations identified here and combined them with previously published results on miR-34a/b/c-regulated pathways in a summarizing model shown in Figure 44. Notably, several of the miR-34 targets displaying elevated expression after *miR-34a/b/c* deletion are involved in transmembrane signal transductions, which also activate the Wnt signaling pathway by inhibition of GSK-3β. Taken together, miR-34a/b/c presumably suppresses intestinal tumorigenesis caused by loss of *Apc* by down-regulating the expression of a large number of pro-tumorigenic factors. In case *miR-34a/b/c* expression is lost or silenced during tumor progression these pathways may be further activated and thereby contribute to CRC progression.
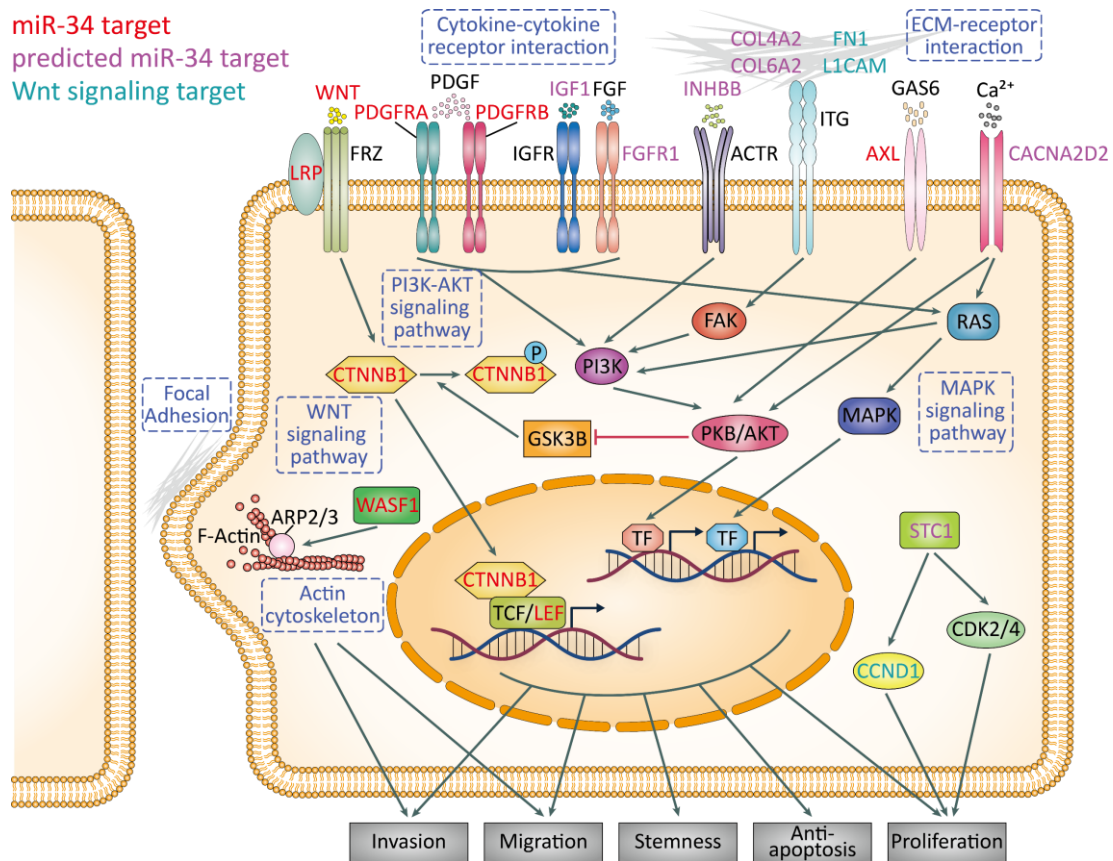
Figure 44.

Summarizing model of regulations and signal transduction events activated by deletion of *miR-34a/b/c* in *Apc*^Min/+ mice identified in this study. In addition, selected previously published (in red) or predicted (in purple) miR-34a/b/c target genes, as well as WNT-regulated factors (in cyan) are depicted.

6. Discussion

We generated transgenic mice with deletion of *miR-34a/b/c* alleles to examine the consequences of *miR-34a/b/c* inactivation for normal development and tumorigenesis. In previous studies, Concepcion *et al.* reported that deletion of *miR-34a/b/c* is compatible with normal development in mice and does not increase spontaneous carcinogenesis [42]. Our results confirmed their findings, since *miR-34a/b/c*-deficient mice did not show any significant changes in lifespan. Interestingly, miR-34a/b/c and miR-449a/b/c constitute a superfamily of miRNAs and contain the same "seed region". Therefore, certain miR-34 functions may be compensated by other miRNAs, such as miR-449, which share a similar seed-matching sequence. In line with this assumption, mice deficient for *miR-34a/b/c* and *miR-449a/b/c* display impaired mucociliary clearance and postnatal mortality, infertility and respiratory dysfunction [45]. However, it should be noted that *miR-449a/b/c* are not induced by p53 and seem to function as oncogenes, as they are induced by E2F transcription factors.

Here we observed changes in the intestinal architecture in *miR-34a/b/c*-deficient mice indicate that miR-34a/b/c have functions in the homeostasis of intestinal epithelial cells. miR-34 may achieve this via some of its target mRNAs, such as *Pdgfra* and *Klf4*, which encode proteins that are known to be involved in the development of the intestine and differentiation of intestinal epithelial cells. Interestingly, *Pdgfra*-deficient mice show fewer and deformed villi [82], and mice with a *Klf4* deletion show a 90% reduction of Goblet cells in the colon [83]. Furthermore, *Sox9*-deficient mice have decreased numbers of Paneth cells [84].

As we expected, the alterations of the small intestinal architecture were retained in $Apc^{Min/+}$ mice after *miR-34a/b/c* loss. Notably, an increased tumor burden and size, and decreased survival were found in *miR-34a/b/c* deletion $Apc^{Min/+}$ mice. The increase in the pool of intestinal stem cells (ISC) in the *miR-34a/b/c*-deficient mice observed here may underlie the increased rate of tumor formation in $Apc^{Min/+}$ mice, since ISC were shown to serve as efficient tumor initiating cells during intestinal tumorigenesis [79]. Paneth cells provide a niche for ISCs and communicate with these via multiple signaling pathways, among them the Delta/NOTCH and Wnt/APC/β-catenin pathways, which are under negative control by miR-34a/b/c [34,54]: e.g. several key components of the Wnt signaling pathway are miR-34a/b/c targets (WNT1, WNT3, LRP6, LEF1, and β-catenin [54,56]. Moreover, GSK-3β, which phosphorylates β-catenin and thereby leads to its poly-ubiquitination and proteasomal degradation, is inhibited by the PKB/AKT and PI3K pathways, which are also under control of miR-34a/b/c. Therefore, the concerted deregulation of the NOTCH and WNT pathways caused by the loss of *miR-34a/b/c* is a likely cause for the increased number of Paneth and stem cells. In support of this scenario, we also noticed an increased tumor organoid formation rate in *miR-34a/b/c$^{-/-}$*; $Apc^{Min/+}$ adenomas as well as an increased accumulation of nuclear β-catenin in the untransformed, epithelial cells of intestinal crypts in *miR-34a/b/c*-deficient $Apc^{Min/+}$ mice. In addition, a recent study suggests that activation of the Wnt/β-catenin pathway correlates with T cell exclusion [85]. Therefore, miR-34 may regulate immune responses through Wnt signaling. In addition, the expression of barrier proteins was decreased in *miR-34a/b/c$^{-/-}$*; $Apc^{Min/+}$ mice (e.g. *Muc1*, *Tff3*, and *Retnlb*). In combination with the decreased

presence of immune cells, these effects of *miR-34a/b/c* loss may contribute, at least in part, to the increased bacterial infiltration observed in *miR-34a/b/c*[-/-]; *Apc*[Min/+] adenomas.

In addition, utilizing whole transcriptomic analysis and subsequent KEGG, GO, and GSEA pathway analysis, we found that the deletion of *miR-34a/b/c* in adenomas leads to the up-regulation of previously described miR-34a/b/c target mRNAs, such as *Pdgfra*, *Pdgfrb*, and *Axl*, which are known to enhance CRC formation [86]. Furthermore, a set of novel, putative miR-34a/b/c target mRNAs (*Wasf1*, *Fgfr1*, *Igf1*, *Stc1*, *Cacna2d2*, *Col6a2*, *Col4a2*, and *Inhbb*), which were reported to be involved in tumorigenesis [81,87-92], was up-regulated in *miR-34a/b/c*-deficient adenomas. The factors encoded by these genes form complex signaling and functional networks (Figure 44): PDGFRA, PDGFRB, FGFR1, AXL and IGF1, which are either ligands or receptors of the tyrosine kinase family, activate the PI3K and MAPK signaling pathway, and thereby promote cell growth, survival, EMT and metastasis [93,88,87,94,95]. Notably, CACNA2D2, a voltage-dependent calcium channel, deregulates calcium homeostasis when ectopically expressed [90]. The resulting calcium release may induce the activation of PKB/AKT and RAS, which are the mediators of the PI3K and MAPK pathways, and eventually promote cell proliferation and angiogenesis [90]. AXL kinase, a receptor tyrosine kinases (RTK) family member, transduces its signal through PI3K pathway and regulates cell survival, aggregation, and proangiogenic behavior [96-98]. INHBB assembles into Activins, which are critical modulators of growth and survival [99,92]. Components of the extracellular matrix (ECM), are commonly deregulated during tumor progression [100] and were found to be up-

regulated putative miR-34a/b/c targets in this study: the collagen COL4A2 is a major structural protein of the basement membrane [101] and COL6A2 has an anchoring function [102]. Both collagens stimulate integrin signaling and are involved in cell growth, angiogenesis, and tumor metastasis [91]. WASF1, a new miR-34a/b/c target characterized here, mediates actin polymerization, lamellipodia formation and plays a critical role in cancer cell migration and invasion [103,104,81]. STC1 is an endocrine regulator of calcium and phosphate homeostasis which promotes cell proliferation and inhibits apoptosis through CCND1 and CDK2/4 [105].

Taken together, miR-34a/b/c presumably act as global regulators to fine tune multiple cellular functions, which are necessary for the homeostasis of intestinal epithelia. Since miR-34a has been shown to form bimodal switches with at least some of its targets [34], the epigenetic silencing of *miR-34a/b/c* during CRC progression may have significant effects on the regulation of these signaling and expression networks which ultimately promote intestinal tumorigenesis. miR-34a/b/c have a multitude of targets in intestinal epithelial and colon cancer cells as shown here and in previous studies [19]. Therefore, it seems plausible that the effects of *miR-34a/b/c* loss are mediated by the combined activity of multiple up-regulated targets and not by one or a few targets.

Our results suggest that a subset of the direct targets of miR-34a/b/c may significantly contribute to human colorectal tumorigenesis since their elevated expression was associated with poor clinical outcomes of CRC patients. Interestingly, decreased *miR-34a* expression, caused by CpG-methylation of its promoter, in combination with increased β-catenin expression are more

significantly associated with liver metastases of CRC than their single deregulation [39]. In the future, the detection of *miR-34a/b/c* silencing and up-regulation of its targets in primary CRC samples may be used for predictive and prognostic purposes. Furthermore, our results suggest that miR-34 mimetics may be used to target multiple key pathways simultaneously and could thereby potentially prevent the emergence of resistance caused by mutations of single pathways. Therefore, miR-34a/b/c replacement therapy may represent a potential option for the treatment of CRC.

7. Summary

The p53-inducible *miR-34a* and *miR-34b/c* genes are frequently silenced in colorectal cancer (CRC). To address the *in vivo* relevance of *miR-34a/b/c* function for suppression of intestinal tumor formation, we generated *Apc*Min/+ mice with deletions of the *miR-34a* and/or *miR-34b/c* genes separately or in combination. Combined deletion of *miR-34a/b/c* increased the number of intestinal stem cells as well as Paneth and Goblet cells, resulting in enlarged intestinal crypts. *miR-34a/b/c*-deficient *Apc*Min/+ mice displayed an increased tumor burden and grade, and decreased survival. *miR-34a/b/c*-deficient adenomas showed elevated proliferation, decreased apoptosis and displayed pronounced bacterial infiltration, which may be due to an observed decrease in infiltrating immune cells and down-regulation of barrier proteins. mRNAs induced in *miR-34a/b/c*-deficient tumors were enriched for miR-34a/b/c seed-matching sites and for mRNAs encoding proteins related to epithelial-mesenchymal transition (EMT), stemness and Wnt signaling. Accordingly, cells explanted from *miR-34a/b/c*-deficient adenomas formed tumor organoids at an increased rate. Several up-regulated miR-34 targets displayed elevated expression in primary human CRCs that was associated with lymph-node metastases (*INHBB, AXL, FGFR1, PDFGRB*) and up-regulation of *INHBB* and *AXL* in primary CRC was associated with poor patient survival. In conclusion, these results show that *miR-34a/b/c* suppress tumor formation caused by loss of *Apc* and control intestinal stem cell and secretory cell homeostasis by down-regulation of multiple target mRNAs.

8. Zusammenfassung

Beim Kolorektalkarzinom werden die p53-induzierbaren *miR-34a* und *miR-34b/c* Gene häufig durch DNA-Methylierung inaktiviert. Um die *in vivo* Relevanz der *miR-34a/b/c* Funktion für die Unterdrückung der Bildung von intestinalen Tumoren zu untersuchen, haben wir *Apc*^{Min/+} Mäuse mit getrennten oder kombinierten Deletionen der *miR-34a* oder *miR-34b/c* Gene generiert. Die kombinierte Deletion von *miR-34a/b/c* erhöhte die Anzahl der Darmstammzellen sowie von Paneth- und Becherzellen, was zu vergrößerten Darmkrypten führte. *miR-34a/b/c*-defiziente *Apc*^{Min/+} Mäuse zeigten vermehrte Tumorbildung, einen erhöhten Malignitätsgrad und ein vermindertes Überleben. Zudem wiesen *miR-34a/b/c*-defiziente Adenome eine erhöhte Proliferation und verminderte Apoptose, sowie eine ausgeprägte bakterielle Infiltration auf. Diese könnte durch die beobachtete Abnahme der infiltrierenden Immunzellen und die verminderte Expression von Barriere-Proteinen erklärt werden. mRNAs welche in *miR-34a/b/c*-defizienten Tumoren verstärkt gebildet wurden, waren für *miR-34a/b/c*-Seed-Matching-Motive angereichert und für mRNAs, die Proteine kodieren, die mit epithelial-mesenchymalen Übergang (EMT), Stammzelligkeit und dem Wnt-Signalweg zusammenhängen. Dementsprechend bildeten Zellen, die aus *miR-34a/b/c*-defizienten Adenomen explantiert wurden, Tumor-Organoide mit einer erhöhten Rate. Mehrere hochregulierte miR-34 Targets zeigten eine erhöhte Expression in primären menschlichen Kolorektalkarzinomen, die mit Lymphknotenmetastasen (*INHBB*, *AXL*, *FGFR1*, *PDFGRB*) assoziiert waren, und die Hochregulierung von *INHBB* und *AXL* in primären Kolorektalkarzinomen war mit geringeren Überleben der Patienten assoziiert.

Zusammenfassend zeigen diese Ergebnisse, dass *miR-34a/b/c* die intestinale Tumorbildung, die durch den Verlust von *Apc* verursacht wird, unterdrückt und die Homöostase von intestinalen Stammzellen und sekretorischen Zellen durch die Inhibition mehrerer Ziel-mRNAs kontrolliert.

9. References

1. Torre, LA, Bray, F, Siegel, RL, Ferlay, J, Lortet-Tieulent, J, & Jemal, A (2015). Global cancer statistics, 2012. *CA Cancer J Clin* **65**: 87-108

2. Vogelstein, B, & Kinzler, KW (2004). Cancer genes and the pathways they control. *Nat Med* **10**: 789-799

3. Hanahan, D, & Weinberg, RA (2000). The hallmarks of cancer. *Cell* **100**: 57-70

4. Fearon, ER, & Vogelstein, B (1990). A genetic model for colorectal tumorigenesis. *Cell* **61**: 759-767

5. Esquela-Kerscher, A, & Slack, FJ (2006). Oncomirs - microRNAs with a role in cancer. *Nat Rev Cancer* **6**: 259-269

6. Di Leva, G, Garofalo, M, & Croce, CM (2014). MicroRNAs in cancer. *Annu Rev Pathol* **9**: 287-314

7. Green, JE, & Hudson, T (2005). The promise of genetically engineered mice for cancer prevention studies. *Nat Rev Cancer* **5**: 184-198

8. Siegel, RL, Miller, KD, & Jemal, A (2017). Cancer Statistics, 2017. *CA Cancer J Clin* **67**: 7-30

9. Kinzler, KW, & Vogelstein, B (1996). Lessons from hereditary colorectal cancer. *Cell* **87**: 159-170

10. Powell, SM, Zilz, N, Beazer-Barclay, Y, Bryan, TM, Hamilton, SR, Thibodeau, SN*, et al.* (1992). APC mutations occur early during colorectal tumorigenesis. *Nature* **359**: 235-237

11. Morin, PJ, Sparks, AB, Korinek, V, Barker, N, Clevers, H, Vogelstein, B*, et al.* (1997). Activation of beta-catenin-Tcf signaling in colon cancer by mutations in beta-catenin or APC. *Science* **275**: 1787-1790

12. Bienz, M, & Clevers, H (2000). Linking colorectal cancer to Wnt signaling. *Cell* **103**: 311-320

13. Baker, SJ, Preisinger, AC, Jessup, JM, Paraskeva, C, Markowitz, S, Willson, JK*, et al.* (1990). p53 gene mutations occur in combination with 17p allelic deletions as late events in colorectal tumorigenesis. *Cancer Res* **50**: 7717-7722

14. Vogelstein, B, Lane, D, & Levine, AJ (2000). Surfing the p53 network. *Nature* **408**: 307-310

15. Bouaoun, L, Sonkin, D, Ardin, M, Hollstein, M, Byrnes, G, Zavadil, J*, et al.* (2016). TP53 Variations in Human Cancers: New Lessons from the IARC TP53 Database and Genomics Data. *Hum Mutat* **37**: 865-876

16. Hermeking, H (2012). MicroRNAs in the p53 network: micromanagement of tumour suppression. *Nat Rev Cancer* **12**: 613-626

17. Hunten, S, Kaller, M, Drepper, F, Oeljeklaus, S, Bonfert, T, Erhard, F*, et al.* (2015). p53-Regulated Networks of Protein, mRNA, miRNA, and lncRNA Expression Revealed by Integrated Pulsed Stable Isotope Labeling With Amino Acids in Cell Culture (pSILAC) and Next Generation Sequencing (NGS) Analyses. *Mol Cell Proteomics* **14**: 2609-2629

18. Suzuki, HI, Yamagata, K, Sugimoto, K, Iwamoto, T, Kato, S, & Miyazono, K (2009). Modulation of microRNA processing by p53. *Nature* **460**: 529-533

19. Rokavec, M, Li, H, Jiang, L, & Hermeking, H (2014). The p53/miR-34 axis in development and disease. *J Mol Cell Biol* **6**: 214-230

20. Tarasov, V, Jung, P, Verdoodt, B, Lodygin, D, Epanchintsev, A, Menssen, A*, et al.* (2007). Differential regulation of microRNAs by p53 revealed by massively parallel sequencing: miR-34a is a p53 target that induces apoptosis and G1-arrest. *Cell Cycle* **6**: 1586-1593

21. Raver-Shapira, N, Marciano, E, Meiri, E, Spector, Y, Rosenfeld, N, Moskovits, N*, et al.* (2007). Transcriptional activation of miR-34a contributes to p53-mediated apoptosis. *Mol Cell* **26**: 731-743

22. Bieging, KT, Mello, SS, & Attardi, LD (2014). Unravelling mechanisms of p53-mediated tumour suppression. *Nat Rev Cancer* **14**: 359-370

23. Bartel, DP (2004). MicroRNAs: genomics, biogenesis, mechanism, and function. *Cell* **116**: 281-297

24. Siemens, H, Jackstadt, R, Hunten, S, Kaller, M, Menssen, A, Gotz, U*, et al.* (2011). miR-34 and SNAIL form a double-negative feedback loop to regulate epithelial-mesenchymal transitions. *Cell Cycle* **10**: 4256-4271

25. Yang, S, Li, Y, Gao, J, Zhang, T, Li, S, Luo, A*, et al.* (2013). MicroRNA-34 suppresses breast cancer invasion and metastasis by directly targeting Fra-1. *Oncogene* **32**: 4294-4303

26. Liu, C, Kelnar, K, Liu, B, Chen, X, Calhoun-Davis, T, Li, H*, et al.* (2011). The microRNA miR-34a inhibits prostate cancer stem cells and metastasis by directly repressing CD44. *Nat Med* **17**: 211-215

27. Christoffersen, NR, Shalgi, R, Frankel, LB, Leucci, E, Lees, M, Klausen, M*, et al.* (2010). p53-independent upregulation of miR-34a during oncogene-induced senescence represses MYC. *Cell Death Differ* **17**: 236-245

28. Zhao, T, Li, J, & Chen, AF (2010). MicroRNA-34a induces endothelial progenitor cell senescence and impedes its angiogenesis via suppressing silent information regulator 1. *Am J Physiol Endocrinol Metab* **299**: E110-116

29. Reya, T, Morrison, SJ, Clarke, MF, & Weissman, IL (2001). Stem cells, cancer, and cancer stem cells. *Nature* **414**: 105-111

30. Ji, Q, Hao, X, Zhang, M, Tang, W, Yang, M, Li, L*, et al.* (2009). MicroRNA miR-34 inhibits human pancreatic cancer tumor-initiating cells. *PLoS One* **4**: e6816

31. Yu, F, Jiao, Y, Zhu, Y, Wang, Y, Zhu, J, Cui, X*, et al.* (2012). MicroRNA 34c gene down-regulation via DNA methylation promotes self-renewal and epithelial-mesenchymal transition in breast tumor-initiating cells. *J Biol Chem* **287**: 465-473

32. Liu, C, & Tang, DG (2011). MicroRNA regulation of cancer stem cells. *Cancer Res* **71**: 5950-5954

33. Bu, P, Chen, KY, Chen, JH, Wang, L, Walters, J, Shin, YJ*, et al.* (2013). A microRNA miR-34a-regulated bimodal switch targets Notch in colon cancer stem cells. *Cell Stem Cell* **12**: 602-615

34. Bu, P, Wang, L, Chen, KY, Srinivasan, T, Murthy, PK, Tung, KL*, et al.* (2016). A miR-34a-Numb Feedforward Loop Triggered by Inflammation Regulates Asymmetric Stem Cell Division in Intestine and Colon Cancer. *Cell Stem Cell* **18**: 189-202

35. Cheng, CY, Hwang, CI, Corney, DC, Flesken-Nikitin, A, Jiang, L, Oner, GM*, et al.* (2014). miR-34 cooperates with p53 in suppression of prostate

cancer by joint regulation of stem cell compartment. *Cell Rep* **6**: 1000-1007

36. Choi, YJ, Lin, CP, Ho, JJ, He, X, Okada, N, Bu, P*, et al.* (2011). miR-34 miRNAs provide a barrier for somatic cell reprogramming. *Nat Cell Biol* **13**: 1353-1360

37. Lodygin, D, Tarasov, V, Epanchintsev, A, Berking, C, Knyazeva, T, Korner, H*, et al.* (2008). Inactivation of miR-34a by aberrant CpG methylation in multiple types of cancer. *Cell Cycle* **7**: 2591-2600

38. Vogt, M, Munding, J, Gruner, M, Liffers, ST, Verdoodt, B, Hauk, J*, et al.* (2011). Frequent concomitant inactivation of miR-34a and miR-34b/c by CpG methylation in colorectal, pancreatic, mammary, ovarian, urothelial, and renal cell carcinomas and soft tissue sarcomas. *Virchows Arch* **458**: 313-322

39. Siemens, H, Neumann, J, Jackstadt, R, Mansmann, U, Horst, D, Kirchner, T*, et al.* (2013). Detection of miR-34a promoter methylation in combination with elevated expression of c-Met and beta-catenin predicts distant metastasis of colon cancer. *Clin Cancer Res* **19**: 710-720

40. Adams, BD, Parsons, C, & Slack, FJ (2016). The tumor-suppressive and potential therapeutic functions of miR-34a in epithelial carcinomas. *Expert Opin Ther Targets* **20**: 737-753

41. Bommer, GT, Gerin, I, Feng, Y, Kaczorowski, AJ, Kuick, R, Love, RE*, et al.* (2007). p53-mediated activation of miRNA34 candidate tumor-suppressor genes. *Curr Biol* **17**: 1298-1307

42. Concepcion, CP, Han, YC, Mu, P, Bonetti, C, Yao, E, D'Andrea, A*, et al.* (2012). Intact p53-dependent responses in miR-34-deficient mice. *PLoS Genet* **8**: e1002797

43. Okada, N, Lin, CP, Ribeiro, MC, Biton, A, Lai, G, He, X*, et al.* (2014). A positive feedback between p53 and miR-34 miRNAs mediates tumor suppression. *Genes Dev* **28**: 438-450

44. Comazzetto, S, Di Giacomo, M, Rasmussen, KD, Much, C, Azzi, C, Perlas, E*, et al.* (2014). Oligoasthenoteratozoospermia and infertility in mice deficient for miR-34b/c and miR-449 loci. *PLoS Genet* **10**: e1004597

45. Song, R, Walentek, P, Sponer, N, Klimke, A, Lee, JS, Dixon, G*, et al.* (2014). miR-34/449 miRNAs are required for motile ciliogenesis by repressing cp110. *Nature* **510**: 115-120

46. Willert, K, & Jones, KA (2006). Wnt signaling: is the party in the nucleus? *Genes Dev* **20**: 1394-1404

47. Liu, C, Li, Y, Semenov, M, Han, C, Baeg, GH, Tan, Y*, et al.* (2002). Control of beta-catenin phosphorylation/degradation by a dual-kinase mechanism. *Cell* **108**: 837-847

48. Moon, RT (2005). Wnt/beta-catenin pathway. *Sci STKE* **2005**: cm1

49. Taketo, MM (2006). Wnt signaling and gastrointestinal tumorigenesis in mouse models. *Oncogene* **25**: 7522-7530

50. Moser, AR, Mattes, EM, Dove, WF, Lindstrom, MJ, Haag, JD, & Gould, MN (1993). ApcMin, a mutation in the murine Apc gene, predisposes to mammary carcinomas and focal alveolar hyperplasias. *Proc Natl Acad Sci U S A* **90**: 8977-8981

51. Luongo, C, Moser, AR, Gledhill, S, & Dove, WF (1994). Loss of Apc+ in intestinal adenomas from Min mice. *Cancer Res* **54**: 5947-5952

52. Bussey, HJ (1979). Familial polyposis coli. *Pathol Annu* **14 Pt 1**: 61-81

53. Moser, AR, Luongo, C, Gould, KA, McNeley, MK, Shoemaker, AR, & Dove, WF (1995). ApcMin: a mouse model for intestinal and mammary tumorigenesis. *Eur J Cancer* **31A**: 1061-1064

54. Kim, NH, Kim, HS, Kim, NG, Lee, I, Choi, HS, Li, XY*, et al.* (2011). p53 and microRNA-34 are suppressors of canonical Wnt signaling. *Sci Signal* **4**: ra71

55. Staal, FJ, Luis, TC, & Tiemessen, MM (2008). WNT signalling in the immune system: WNT is spreading its wings. *Nat Rev Immunol* **8**: 581-593

56. Kaller, M, Liffers, ST, Oeljeklaus, S, Kuhlmann, K, Roh, S, Hoffmann, R*, et al.* (2011). Genome-wide characterization of miR-34a induced changes in protein and mRNA expression by a combined pulsed SILAC and microarray analysis. *Mol Cell Proteomics* **10**: M111 010462

57. Amann, RI, Binder, BJ, Olson, RJ, Chisholm, SW, Devereux, R, & Stahl, DA (1990). Combination of 16S rRNA-targeted oligonucleotide probes with flow cytometry for analyzing mixed microbial populations. *Appl Environ Microbiol* **56**: 1919-1925

58. Vogelstein, B, & Kinzler, KW (1999). Digital PCR. *Proc Natl Acad Sci U S A* **96**: 9236-9241

59. Sato, T, Stange, DE, Ferrante, M, Vries, RG, Van Es, JH, Van den Brink, S*, et al.* (2011). Long-term expansion of epithelial organoids from human

colon, adenoma, adenocarcinoma, and Barrett's epithelium. *Gastroenterology* **141**: 1762-1772

60. Xue, X, & Shah, YM (2013). In vitro organoid culture of primary mouse colon tumors. *J Vis Exp*: e50210

61. Schwitalla, S, Ziegler, PK, Horst, D, Becker, V, Kerle, I, Begus-Nahrmann, Y*, et al.* (2013). Loss of p53 in enterocytes generates an inflammatory microenvironment enabling invasion and lymph node metastasis of carcinogen-induced colorectal tumors. *Cancer Cell* **23**: 93-106

62. Rokavec, M, Oner, MG, Li, H, Jackstadt, R, Jiang, L, Lodygin, D*, et al.* (2014). IL-6R/STAT3/miR-34a feedback loop promotes EMT-mediated colorectal cancer invasion and metastasis. *J Clin Invest* **124**: 1853-1867

63. Livak, KJ, & Schmittgen, TD (2001). Analysis of relative gene expression data using real-time quantitative PCR and the 2(-Delta Delta C(T)) Method. *Methods* **25**: 402-408

64. Hirsch, FR, Varella-Garcia, M, Bunn, PA, Jr., Di Maria, MV, Veve, R, Bremmes, RM*, et al.* (2003). Epidermal growth factor receptor in non-small-cell lung carcinomas: correlation between gene copy number and protein expression and impact on prognosis. *J Clin Oncol* **21**: 3798-3807

65. Johansson, AC, Visse, E, Widegren, B, Sjogren, HO, & Siesjo, P (2001). Computerized image analysis as a tool to quantify infiltrating leukocytes: a comparison between high- and low-magnification images. *J Histochem Cytochem* **49**: 1073-1079

66. Risso, D, Ngai, J, Speed, TP, & Dudoit, S (2014). Normalization of RNA-seq data using factor analysis of control genes or samples. *Nat Biotechnol* **32**: 896-902

67. Kallio, MA, Tuimala, JT, Hupponen, T, Klemela, P, Gentile, M, Scheinin, I*, et al.* (2011). Chipster: user-friendly analysis software for microarray and other high-throughput data. *BMC Genomics* **12**: 507

68. Huang da, W, Sherman, BT, & Lempicki, RA (2009). Bioinformatics enrichment tools: paths toward the comprehensive functional analysis of large gene lists. *Nucleic Acids Res* **37**: 1-13

69. Subramanian, A, Tamayo, P, Mootha, VK, Mukherjee, S, Ebert, BL, Gillette, MA*, et al.* (2005). Gene set enrichment analysis: a knowledge-based approach for interpreting genome-wide expression profiles. *Proc Natl Acad Sci U S A* **102**: 15545-15550

70. Lewis, BP, Burge, CB, & Bartel, DP (2005). Conserved seed pairing, often flanked by adenosines, indicates that thousands of human genes are microRNA targets. *Cell* **120**: 15-20

71. Cancer Genome Atlas, N (2012). Comprehensive molecular characterization of human colon and rectal cancer. *Nature* **487**: 330-337

72. Grossman, RL, Heath, AP, Ferretti, V, Varmus, HE, Lowy, DR, Kibbe, WA*, et al.* (2016). Toward a Shared Vision for Cancer Genomic Data. *N Engl J Med* **375**: 1109-1112

73. Li, B, & Dewey, CN (2011). RSEM: accurate transcript quantification from RNA-Seq data with or without a reference genome. *BMC Bioinformatics* **12**: 323

74. Lee, SH, Hu, LL, Gonzalez-Navajas, J, Seo, GS, Shen, C, Brick, J*, et al.* (2010). ERK activation drives intestinal tumorigenesis in Apc(min/+) mice. *Nat Med* **16**: 665-670

75. Love, MI, Huber, W, & Anders, S (2014). Moderated estimation of fold change and dispersion for RNA-seq data with DESeq2. *Genome Biol* **15**: 550

76. Robinson, MD, McCarthy, DJ, & Smyth, GK (2010). edgeR: a Bioconductor package for differential expression analysis of digital gene expression data. *Bioinformatics* **26**: 139-140

77. Munoz, J, Stange, DE, Schepers, AG, van de Wetering, M, Koo, BK, Itzkovitz, S*, et al.* (2012). The Lgr5 intestinal stem cell signature: robust expression of proposed quiescent '+4' cell markers. *EMBO J* **31**: 3079-3091

78. Merlos-Suarez, A, Barriga, FM, Jung, P, Iglesias, M, Cespedes, MV, Rossell, D*, et al.* (2011). The intestinal stem cell signature identifies colorectal cancer stem cells and predicts disease relapse. *Cell Stem Cell* **8**: 511-524

79. Barker, N, Ridgway, RA, van Es, JH, van de Wetering, M, Begthel, H, van den Born, M*, et al.* (2009). Crypt stem cells as the cells-of-origin of intestinal cancer. *Nature* **457**: 608-611

80. Garofalo, M, Jeon, YJ, Nuovo, GJ, Middleton, J, Secchiero, P, Joshi, P*, et al.* (2013). MiR-34a/c-Dependent PDGFR-alpha/beta Downregulation Inhibits Tumorigenesis and Enhances TRAIL-Induced Apoptosis in Lung Cancer. *PLoS One* **8**: e67581

81. Zhang, J, Zhou, S, Tang, L, Shen, L, Xiao, L, Duan, Z*, et al.* (2013). WAVE1 gene silencing via RNA interference reduces ovarian cancer cell invasion, migration and proliferation. *Gynecol Oncol* **130**: 354-361

82. Karlsson, L, Lindahl, P, Heath, JK, & Betsholtz, C (2000). Abnormal gastrointestinal development in PDGF-A and PDGFR-(alpha) deficient mice implicates a novel mesenchymal structure with putative instructive properties in villus morphogenesis. *Development* **127**: 3457-3466

83. Katz, JP, Perreault, N, Goldstein, BG, Lee, CS, Labosky, PA, Yang, VW*, et al.* (2002). The zinc-finger transcription factor Klf4 is required for terminal differentiation of goblet cells in the colon. *Development* **129**: 2619-2628

84. Mori–Akiyama, Y, Van den Born, M, Van Es, JH, Hamilton, SR, Adams, HP, Zhang, J*, et al.* (2007). SOX9 is required for the differentiation of paneth cells in the intestinal epithelium. *Gastroenterology* **133**: 539-546

85. Corrales, L, Matson, V, Flood, B, Spranger, S, & Gajewski, TF (2017). Innate immune signaling and regulation in cancer immunotherapy. *Cell Res* **27**: 96-108

86. Craven, RJ, Xu, LH, Weiner, TM, Fridell, YW, Dent, GA, Srivastava, S*, et al.* (1995). Receptor tyrosine kinases expressed in metastatic colon cancer. *Int J Cancer* **60**: 791-797

87. Grose, R, & Dickson, C (2005). Fibroblast growth factor signaling in tumorigenesis. *Cytokine Growth Factor Rev* **16**: 179-186

88. Olivo-Marston, SE, Hursting, SD, Lavigne, J, Perkins, SN, Maarouf, RS, Yakar, S*, et al.* (2009). Genetic reduction of circulating insulin-like growth

factor-1 inhibits azoxymethane-induced colon tumorigenesis in mice. *Mol Carcinog* **48**: 1071-1076

89. Tamura, S, Oshima, T, Yoshihara, K, Kanazawa, A, Yamada, T, Inagaki, D*, et al.* (2011). Clinical significance of STC1 gene expression in patients with colorectal cancer. *Anticancer Res* **31**: 325-329

90. Warnier, M, Roudbaraki, M, Derouiche, S, Delcourt, P, Bokhobza, A, Prevarskaya, N*, et al.* (2015). CACNA2D2 promotes tumorigenesis by stimulating cell proliferation and angiogenesis. *Oncogene* **34**: 5383-5394

91. Worthley, DL, Giraud, AS, & Wang, TC (2010). The extracellular matrix in digestive cancer. *Cancer Microenviron* **3**: 177-185

92. Togashi, Y, Kogita, A, Sakamoto, H, Hayashi, H, Terashima, M, de Velasco, MA*, et al.* (2015). Activin signal promotes cancer progression and is involved in cachexia in a subset of pancreatic cancer. *Cancer Lett* **356**: 819-827

93. Carnero, A (2010). The PKB/AKT pathway in cancer. *Curr Pharm Des* **16**: 34-44

94. Heinrich, MC, Corless, CL, Duensing, A, McGreevey, L, Chen, CJ, Joseph, N*, et al.* (2003). PDGFRA activating mutations in gastrointestinal stromal tumors. *Science* **299**: 708-710

95. Steller, EJ, Raats, DA, Koster, J, Rutten, B, Govaert, KM, Emmink, BL*, et al.* (2013). PDGFRB promotes liver metastasis formation of mesenchymal-like colorectal tumor cells. *Neoplasia* **15**: 204-217

96. Bellosta, P, Costa, M, Lin, DA, & Basilico, C (1995). The receptor tyrosine kinase ARK mediates cell aggregation by homophilic binding. *Mol Cell Biol* **15**: 614-625

97. Fridell, YW, Jin, Y, Quilliam, LA, Burchert, A, McCloskey, P, Spizz, G*, et al.* (1996). Differential activation of the Ras/extracellular-signal-regulated protein kinase pathway is responsible for the biological consequences induced by the Axl receptor tyrosine kinase. *Mol Cell Biol* **16**: 135-145

98. Suleiman, L, Negrier, C, & Boukerche, H (2013). Protein S: A multifunctional anticoagulant vitamin K-dependent protein at the crossroads of coagulation, inflammation, angiogenesis, and cancer. *Crit Rev Oncol Hematol* **88**: 637-654

99. Brown, CW, Li, L, Houston-Hawkins, DE, & Matzuk, MM (2003). Activins are critical modulators of growth and survival. *Mol Endocrinol* **17**: 2404-2417

100. Lu, P, Weaver, VM, & Werb, Z (2012). The extracellular matrix: a dynamic niche in cancer progression. *J Cell Biol* **196**: 395-406

101. Poschl, E, Schlotzer-Schrehardt, U, Brachvogel, B, Saito, K, Ninomiya, Y, & Mayer, U (2004). Collagen IV is essential for basement membrane stability but dispensable for initiation of its assembly during early development. *Development* **131**: 1619-1628

102. Keene, DR, Engvall, E, & Glanville, RW (1988). Ultrastructure of type VI collagen in human skin and cartilage suggests an anchoring function for this filamentous network. *J Cell Biol* **107**: 1995-2006

103. Stradal, TE, Rottner, K, Disanza, A, Confalonieri, S, Innocenti, M, & Scita, G (2004). Regulation of actin dynamics by WASP and WAVE family proteins. *Trends Cell Biol* **14**: 303-311

104. Sarmiento, C, Wang, W, Dovas, A, Yamaguchi, H, Sidani, M, El-Sibai, M*, et al.* (2008). WASP family members and formin proteins coordinate

regulation of cell protrusions in carcinoma cells. *J Cell Biol* **180**: 1245-1260

105. Du, YZ, Gu, XH, Cheng, SF, Li, L, Liu, H, Hu, LP*, et al.* (2016). The oncogenetic role of stanniocalcin 1 in lung adenocarcinoma: a promising serum candidate biomarker for tracking lung adenocarcinoma progression. *Tumour Biol* **37**: 5633-5644

10. Acknowledgements

I would like to express my gratitude to all those who helped me during this work.

My deepest gratitude goes first and foremost to Prof. Heiko Hermeking, my supervisor, for his continuous support and guidance of my doctoral study, related research and the completion of this thesis, as well as his advice, scientific input and ideas which helped me in all the time of research.

Moreover, I would like to thank all former and present members of the group for helpfulness and valuable support throughout the past years. In particular, I would like to thank Dr. Matjaz Rokavec for initial help with setting up the $Apc^{Min/+}$ mouse cohorts, Dr. Markus Kaller for advice on bioinformatics analyses and Dr. Peter Jung for interesting discussions. In addition, I would like to express my gratitude to Dr. Lei Shi, Dr. Yina Zhang, Huihui Li, Xiaolong Shi and Kecheng Lei for their great scientific help and support.

Furthermore, I am grateful to Prof. Alexander Nikitin for providing *miR-34b/c*$^{fl/fl}$ mice, Dr. Marlon Schneider for $Apc^{Min/+}$ mice and Prof. Hans Clevers for the *Olfm4* plasmid. I would like to thank Ursula Götz for her great technical support and helping me work out all the daily challenges in the lab.

Additionally, I would like to thanks my thesis committee, for taking the time and effort to evaluate my work.

Last but not least, I would like to thank my parents for unwavering love and support. Words are powerless to express my love to them.

Curriculum Vitae

Longchang Jiang, M. Sc. Medical Science, *December 28th, 1985 in China

Education:

Sep. 2008 – Jun. 2011: Master of Medical Science 2011
Supervisor: Prof. M.D. Xincai Qu
Union Hospital affiliated to Tongji Medical College,
Huazhong University of Science & Technology
(HUST), Wuhan, China

Sep. 2005 – Jun. 2009: Bachelor of Arts 2009
School of Foreign Language, HUST, Wuhan, China

Sep. 2004 – Jun. 2008: Bachelor of Medicine 2008
Tongji Medical College, HUST, Wuhan, China

Research Experience:

Experimental and Molecular Pathology,
Pathology Institute, Medical Faculty, LMU, Germany

Oct. 2011 – Present: Dr. rer. nat. thesis, Supervisor: Prof. Heiko Hermeking
"Genetic analysis of *miR-34a* and *miR-34b/c* functions
in a mouse model of familial adenomatous polyposis"
Supported by CSC fellowship (2011-2015)

Union Hospital affiliated to Tongji Medical College, HUST, China

Jul. 2009 – Jun. 2011: Master Student, Research Team Member
"Screening organ–specific metastasis gene of breast
cancer and induction site–specific metastasis"
Supported by Nation Natural Science Foundation of
China

Dec. 2008 – Jun. 2009: Master Student, Research Team Member
 "The effect of *Reck* gene after liver transplantation in
rats"
Supported by Ministry of Education of China